Journal of Structural Geology 205 (2026) 105650

Contents lists available at ScienceDirect

Journal of Structural Geology

journal homepage: www.elsevier.com/locate/jsg

Inherited rift faults as Drivers of orogenic complexity: The case of the Amora Fault System, central Southern Alps (N Italy)

Martina Rocca *, Stefano Zanchetta, Andrea Zanchi

Dipartimento di Scienze dell'Ambiente e della Terra, Università degli Studi di Milano Bicocca, Piazza della Scienza 4, 20126, Milan, Italy

ARTICLE INFO

Keywords:
Rift inheritance
Fault reactivation
Basin inversion
Alpine orogeny
Southern Alps

ABSTRACT

Studying structural inversion phenomena is essential for reconstructing fold-and-thrust belt evolution and understanding how pre-existing structures influence their final architecture. In this study, we investigate the tectonic evolution of the Amora Fault System in the central Southern Alps, a Jurassic rift-related structure repeatedly reactivated during Alpine orogenesis. We reconstruct the multiphase history of faulting through detailed structural mapping, paleostress analyses, and microstructural analysis of fracture-filled carbonates, integrated with analogue model comparisons. The Amora Fault System initiated as a long-lived N–S-striking normal fault system during the Early–Middle Jurassic rifting, followed by renewed post-rift reactivation in the Late Jurassic-Early Cretaceous. Subsequent Alpine compression (Late Cretaceous–Eocene) led to the development of the S-verging Albino Thrust, strike-slip reactivation of Jurassic normal faults, and mid-Eocene magmatism accompanied by emplacement of E–W-trending andesitic dikes and associated faulting. Paleostress reconstructions reveal progressive changes in stress orientation, with a vertical σ_1 and an E-W trending σ_3 during the Jurassic, a N-S σ_3 during the mid-Eocene magmatism, and a horizontal N–S-directed σ_1 during Alpine compression. The evolution of the Amora Fault System highlights the interplay between structural inheritance, thermal weakening, and stress field reorientation in controlling fault reactivation, thrust segmentation, and deformation partitioning. More broadly, this study illustrates how inherited rift structures govern the architecture of orogenic belts, generating complex along-strike thrust geometries and multiphase deformation patterns. These results contribute to a better understanding of fault system evolution across rift–orogen cycles, with implications for tectonic reconstruction and seismic hazard assessment.

1. Introduction

Basin inversion has been extensively studied over the past few decades (Bally, 1983; Buchanan and Buchanan, 1995; Cooper et al., 1989; Harding, 1985; Ziegler, 1987). This strong interest stems from the significant implications of upper crustal reactivation of pre-existing structures, including hydrocarbon exploration and production (e.g., Lyon et al., 2007; Manzocchi et al., 2010; Morley, 1995; Wang et al., 2021), and, more recently, applications in seismic hazard assessment (Curzi et al., 2024; Fonseca, 1988; Hecker et al., 2021; Sibson and Ghisetti, 2018; Tarayoun et al., 2019; Wedmore et al., 2020), geothermal energy (Bertrand et al., 2018; Brogi, 2008; Dávalos-Elizondo and Laó-Dávila, 2023; Weert et al., 2024), mineral exploration (Rowland and Sibson, 2004), and CO_2 storage (e.g., Andrés et al., 2016; Gunter et al., 2004; Hitchon et al., 1999; Kampman et al., 2012; Tueckmantel et al., 2012). Consequently, many studies have focused on the reactivation of normal faults during basin inversion (e.g., Beauchamp et al., 1999; Buiter et al., 2009; Cooper and Warren, 2020; Coward et al., 1991; Pace et al., 2014; Tavani et al., 2011, 2021; Turner and Williams, 2004), whereas studies on the strike-slip reactivation of normal faults remain limited (e.g., Kim et al., 2001; Rotevatn and Peacock, 2018; Turner, 1997). Nevertheless, understanding strike-slip reactivation in sedimentary basins is essential, as it directly influences fluid flow pathways.

The influence of rift-related faults on orogenic evolution has been widely documented across the Alps (e.g., Butler et al., 2006; Coward et al., 1991; Manatschal et al., 2022a; Mohn et al., 2011; Schmid et al., 2004), where structural inheritance has played a key role in controlling the localization and geometry of thrusts, back-thrusts, and transpressional faults. Most of these studies have focused either on the compressional reactivation of inherited rift-related faults (i.e., where the shortening direction is orthogonal to the fault array), or on strike-slip reactivation along structures inherited from the distal margin of the

* Corresponding author.
E-mail addresses: martina.rocca@unimib.it (M. Rocca), stefano.zanchetta@unimib.it (S. Zanchetta), andrea.zanchi@unimib.it (A. Zanchi).

https://doi.org/10.1016/j.jsg.2026.105650
Received 25 November 2025; Received in revised form 9 February 2026; Accepted 9 February 2026
Available online 10 February 2026

Western Alps. A number of studies have addressed strike-slip reactivation of inherited faults in the Southalpine domain (Bertotti, 1991; Castellarin et al., 2006; Curzi et al., 2023; Schönborn, 1990, 1992; Zampieri and Massironi, 2007; Zanchetta et al., 2015; Zanchi et al., 1990, 2012). However, only a few provide a comprehensive characterization of the different tectonic phases, supported by integrated macro- and microstructural analyses of small-scale brittle deformation. The analysis of secondary faults in fold-and-thrust belts is fundamental for documenting and quantifying early tectonic events, as major pre-orogenic faults are often difficult to identify. Recognizing these structures is therefore crucial, as they exert a strong control on the structural and mechanical evolution of fold-and-thrust belts (Brown et al., 2017; Homberg et al., 2002; Lacombe et al., 2019; Mazzotti and Gueydan, 2018; Tavani et al., 2025).Recent analogue models have demonstrated how inversion of extensional basins can result in strike-slip reactivation of normal faults (Del Ventisette et al., 2006; Samsu et al., 2023; Sieberer et al., 2023, 2025) and have shown how inherited structures influence the final architecture of orogens, producing complex geometries. These models illustrate that fault inversion is highly dependent on the orientation of pre-existing faults and crustal discontinuities, as well as on the rheology of the involved rocks.In this study, we analyse the Amora Fault System, a Jurassic rift-related normal fault network in the central Southern Alps (cSA) that played a key role in partitioning deformation during the Alpine orogeny. This fault system represents an ideal case study for several reasons: (a) the main structure—the Amora Fault (AF)—is one of the very few Jurassic-inherited structures in the Southern Alps that preserved clear syn-sedimentary features; (b) within the damage zone of the Amora Fault, small-scale brittle deformations (secondary faults, tension gashes, and extension veins) are widespread and displays well-defined crosscutting relationships, allowing a detailed reconstruction of the deformation chronology of both pre-orogenic and orogenic tectonic stages; and (c) the Amora Fault System provides an excellent natural example for investigating the role of pre-existing faults, as it was reactivated multiple times during Jurassic rifting (Rocca et al., 2024) and later during Alpine compression (Zanchetta et al., 2015; Zanchi et al., 1990).

In a previous study by Zanchi et al. (1990), the authors proposed a broad reconstruction of the evolution of the Amora Fault. However, the characterization of superimposed tectonic stages, as well as the roles of inherited structures, rheology, and geothermal gradients, was not fully addressed or was lacking. This absence of constraints limits our understanding of how inherited structures influence subsequent deformation, reactivation, and inversion processes in the central Southern Alps. We aim to fill this gap by integrating multi-scale and paleostress analyses with microstructural study of carbonate-filled fractures. This approach allows us to reconstruct the polyphase tectonic evolution of the Amora Fault System, providing for the first time a detailed documentation of its Early Jurassic origin and its complex Alpine reactivation, supported by quantitative paleostress analyses and constraints on deformation distribution. Finally, by comparing our structural data with existing analogue models of inverted extensional basins, the Amora Fault System serves as a robust natural example for analogue and numerical modelling of fault reactivation during orogenesis.

2. Geological setting

2.1. Tectono-sedimentary evolution of the central southern Alps

The central Southern Alps (cSA; Fig. 1a) started to form in the Late Cretaceous (Schönborn, 1992; Zanchetta et al., 2012, 2015) as the south-verging retro-belt of the European Alps. The cSA is separated from the north-verging portion of the Alps by the Periadriatic Fault, a transpressive orogen-scale structure active since the late Paleogene ((Müller et al., 2001; Schmid et al., 1989; Schönborn, 1992; Zanchetta et al., 2023). The cSA, extending between Lake Como and the Adamello Batholith, is characterized by a thick-skinned fold-and-thrust belt (Carminati, 2009; Forcella and Jadoul, 2000; Schönborn, 1992) that involves the polyphase Variscan basement (Spalla and Gosso, 1999; Zanchetta et al., 2015) and its upper Paleozoic to Cenozoic sedimentary cover.

The cSA experienced a polyphase evolution, starting from the end of the Variscan orogeny (Late Carboniferous–Early Permian), during a period of major crustal reorganization across Europe taking to the collapse of the Variscan belt, which resulted in the formation of fault-controlled troughs filled with continental deposits (Gallo et al., 2017; Le Pichon et al., 2021; Locchi et al., 2022; Ménard and Molnar, 1988; Muttoni et al., 2009; Pohl et al., 2018).

During the Triassic marine transgression, the cSA was involved in several attempted rifting events (Berra and Carminati, 2009; Bertotti et al., 1993; Winterer and Bosellini, 1981) culminating in the Late Triassic-Early Jurassic opening of the Alpine Tethys. During and shortly after the deposition of the 1000 thick lower Norian Dolomia Principale, the resulting carbonate platform was affected by normal faulting with the formation of intraplatform basins controlled by syn-sedimentary faults (Berra et al., 2009, 2010; Berra and Jadoul, 1996; Bertotti et al., 1993; Jadoul et al., 1994; Winterer and Bosellini, 1981). Syn-sedimentary faults are marked by slope breccias in the Dolomia Principale Formation, juxtaposed to structural highs characterized by marginal facies (Berra, 2023; Berra et al., 2009; Berra and Jadoul, 1996; Jadoul et al., 1992). Syn-sedimentary faults border intraplatform basins filled with dark limestones and dolostones (Dolomie Zonate Formation), and organic-rich black mudstones and marls (Zorzino Limestone), that are in turn covered by black shales and marls (Riva di Solto Shale; Casati and Gnaccolini, 1967; Jadoul et al., 1992, 1994), sealing the early Norian normal faults (Fig. 1; Bernoulli et al., 1967; Berra et al., 2009). A gradual reestablishment of carbonate sedimentation is suggested by the deposition of the Zu Limestone during Rhaetian, smoothing the topography inherited from the Norian extension (Berra et al., 2009; Casati and Gnaccolini, 1967).

At the beginning of the Early Jurassic, the Southern Alps were divided in structural domains marked by different subsidence rates, from west to east: the Cusio-Biella-Canavese zone, the Lombardian Basin (cSA area), the Trento High, the Belluno Basin and Friuli Platform (Berra and Carminati, 2009; Bertotti et al., 1993; Winterer and Bosellini, 1981). At the Triassic-Jurassic boundary, the last carbonate platform successions, characterized by massive oolitic limestones (Albenza Formation; Jadoul and Galli, 2008; Ronchi et al., 2011), were followed by bioclastic cherty limestones (Sedrina Limestone; Jadoul and Galli, 2008) deposited throughout the entire Lombardian Basin (Berra and Carminati, 2009; Galli et al., 2005; Jadoul and Galli, 2008). From the late Hettangian, the Lombardian Basin experienced high subsidence rates (200-300 m/Ma) and became further fragmented into fault-controlled half-graben basins (e.g., Generoso and Sebino basins; Fig. 1b) and paleo-highs (e.g., Mt. Cavallo, Botticino highs; Fig. 1b) due to the opening of the Alpine Tethys (Bertotti et al., 1993; Gaetani, 1975; Winterer and Bosellini, 1981). The resulting half-grabens were filled with thick marly turbidites (Moltrasio Limestone; Gaetani, 1975), characterized by rapid thickness changes, sedimentary breccias reworking older units, and m-thick slumps near structural highs and intermediate highs bounded by N-S listric syn-sedimentary extensional faults (Berra and Carminati, 2009; Rocca et al., 2024). The Moltrasio Limestone was capped by upper Pliensbachian grey and marly limestones with chert nodules, intercalated nodular marls and shales (Domaro Limestone). The peak of rifting activity in the Lombardian Basin occurred during the Sinemurian-Pliensbachian, after which subsidence rates drastically decreased, and most of rifting activity shifting westward to the Canavese zone (Berra and Carminati, 2009; Bertotti et al., 1993; Manatschal et al., 2022b; Santantonio and Carminati, 2011). Tectonic activity decreased in the Lombardian Basin, continuing with several pulses at least until Bathonian (Rocca et al., 2024), when mantle exhumation occurred in the Ivrea-Verbano zone (165 ± 7 Ma; Corvò et al., 2025; Ewing et al., 2015; Ferrando et al., 2004). This was further supported by renewed

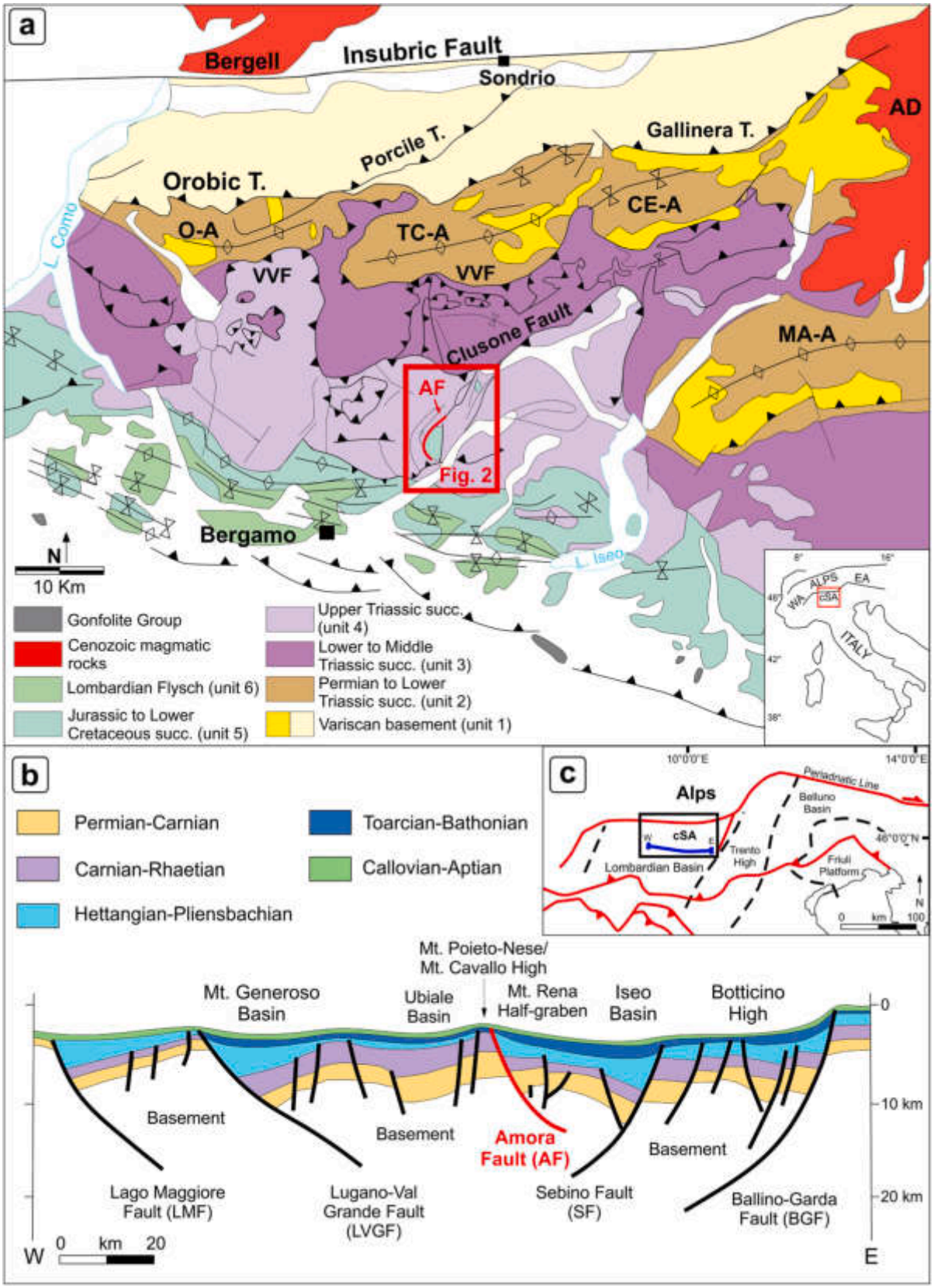

Fig. 1. **(a)** Geological scheme of the central Southern Alps (cSA), modified from Zanchetta et al. (2015). The red square shows the location represented in the map of Fig. 2. AD - Adamello Batholith; CE-A - Cedegolo Anticline; MA-A - Monte Alto Anticline; TC-A -Trabuchello-Cà Bianca Anticline; O-A - Orobic Anticline; and VVF - Valtorta-Valcanale Fault. **(b)** Lombardian Basin configuration at the end of the Early Cretaceous (modified from Berra and Carminati, 2009). CG - Concesio Group and So - Sogno Formation. **(c)** Tectonic framework of Northern Italy. Dashed lines mark Mesozoic rift-related basin and high boundaries. The black rectangle highlights the central Southern Alps (cSA), and the blue W–E line shows the position of section (b). After Berra and Carminati (2009). (For interpretation of the references to colour in this figure legend, the reader is referred to the Web version of this article.)

tectonic activity along the Ballino-Garda fault system in the eastern Lombardian Basin (Sebino basin), where calcareous turbidites of the Concesio Group (early Toarcian-Bathonian; Bersezio et al., 1996) accumulated in the eastern portion of the Lombardian Basin up to the Mt. Cavallo high (Bersezio et al., 1996; Winterer and Bosellini, 1981).

Around Late Jurassic times, sedimentation rates were low, and pelagic sedimentation (Selcifero Lombardo Group) prevailed across much of the Southern Alps due to post-break-up subsidence related to lithospheric cooling with the deposition of the Radiolarites and Rosso ad Aptici formations (Berra and Carminati, 2009; Bertotti et al., 1993; Winterer and Bosellini, 1981). They were followed upsection (Carminati et al., 2010; Fantoni and Scotti, 2003) by pelagic limestones (Maiolica Formation; Petti and Falorni, 2007).

During Late Jurassic to Early Cretaceous, along the Ballino-Garda fault system a renovation of faulting occurred, as testified by submarine slide breccias intercalated in pelagic limestone near the base of the Garda escarpment (Castellarin, 1972; Winterer and Bosellini, 1981). Moreover, the heterochronous distribution of mass gravity deposits and their close relationship with the presence of erosional unconformities further suggests a renewed tectonic activity in the Lombardian Basin (Bersezio et al., 2002).

At the end of Early Cretaceous (Albian), a significant shift of the basin's paleogeography occurred in the Lombardian Basin, with the onset of black shale deposition and a reorganization of troughs from a N-S to a E-W orientation (Berra and Carminati, 2009; Bersezio et al., 1993; Winterer and Bosellini, 1981). This period also marks the first influx of terrigenous material into the basin, with siliciclastic turbidites sourced from outside the basin, including metamorphic rock fragments mainly sourced from areas uplifted during the closure of the oceanic basins between Adria and the European plates to the north (Bernoulli and Winkler, 1990; Bersezio et al., 1993, 2009).

2.2. Alpine tectonic evolution of the central southern Alps

The Late Cretaceous tectonic activity in the cSA (Brack, 1981, 1984; Doglioni and Bosellini, 1987; Laubscher, 1985; Schönborn, 1992; Zanchetta et al., 2012, 2015), marking the onset of the Eoalpine orogeny, is documented by pseudotachylytes formed along the Orobic Thrusts, active from 79.9 ± 1.8 Ma (Zanchetta et al., 2011). This event is attributed to the first pre-Adamello compression (Brack, 1981; Zanchetta et al., 2015), stacking the Variscan basement upon the sedimentary cover along a south vergent thrust system (Schönborn, 1992; Zanchetta et al., 2015). During this stage, most of the Lower to Middle Triassic units between the Valtorta-Val Canale Fault and the Clusone Fault were stacked southward, following a break-forward sequence (D'Adda et al., 2011; Zanchetta et al., 2015). Additionally, ENE-WSW to N-S striking structures inherited from Permian and Late Triassic-Jurassic extension were partially inverted, contributing to the high structural complexity of the cSA (Zanchetta et al., 2015; Zanchi et al., 2012). The beginning of orogenic activity is also testified in the cSA retro-foredeep by the deposition of thick Upper Cretaceous turbidite successions with megabeds accompanied by unconformities suggesting syn-tectonic sedimentation (Bersezio et al., 1994).

The second pre-Adamello compressional stage (late Paleocene – middle Eocene; Zanchetta et al., 2015) involved deeper structural levels of the cSA, resulting in the southward propagation of the Orobic Anticlines, northward backthrusting along the Valtorta-Val Canale Fault and the Clusone Fault, and a gentle southward tilting of the previous main thrust surfaces (Zanchetta et al., 2015; Zanchi et al., 2012).

Shortly after the emplacement of the Adamello batholith (42-39 Ma; Callegaro and Brack, 2002), and andesitic dikes intruding thrust stacks of the Triassic thrust sheets (42-38 Ma; Bergomi et al., 2015; D'Adda et al., 2011), compression resumed in the Oligocene (Zanchetta et al., 2015) due to the southward migration of the deformation front in a break-forward sequence. By the end of Miocene, southward passive transport of Triassic thrust-sheets and out-of-sequence reactivations of inherited structures occurred (Fantoni et al., 2004; Schönborn, 1992), together with deformations along the Insubric Line and the Giudicarie Fault System (Garzanti and Malusà, 2008; Schmid et al., 1989; Zanchetta et al., 2023). Strike-slip reactivations are also documented within the cSA along the Orobic-Porcile-Gallinera thrust system and the Tonale Line during and after the emplacement of the Adamello batholith (Mittempergher et al., 2021; Pennacchioni, 2005; Stipp et al., 2004; Zanchetta et al., 2015).

During the early Oligocene up to Late Miocene, a deep-water clastic complex was deposited into the Southalpine Cenozoic retro-foredeep (Gonfolite Lombarda), fed by the growing post-collisional Alpine belt. The Oligo-Miocene clastic wedge was involved in the southward propagation of the cSA thrusts (Fantoni et al., 2004; Malusà et al., 2011), reflecting the indentation of Europe and Adria (Bernoulli et al., 1967; Zanchetta et al., 2023), still partially active also during the Quaternary (Fantoni et al., 2004; Zanchi et al., 2022).

2.3. The Amora Fault System

The Amora Fault System is a 12 km N-S striking fault system developed on the west side of the Seriana Valley (Bergamo, Italy). It is bounded to the north by the Clusone Fault and to the south by the Albino Thrust (Fig. 2). The main fault of the system is the Amora Fault (AF), a 5 km N-S striking normal fault bordering a Jurassic half-graben basin, juxtaposing the Upper Triassic succession in the footwall to the Lower Jurassic succession in the hanging wall (Fig. 2).

The structural evolution of the Amora Fault System was previously studied by Zanchi et al. (1990), who identified three main deformative events. (1) The oldest structures are N-S striking normal faults, exhibiting offsets of several hundred meters related to the Early Jurassic E-W extension connected to the proximal domain of the Alpine Tethys rift. In the Amora area, the presence of a reduced lowermost Jurassic succession (Bersezio et al., 2012) exposed on top of Mt. Poieto (Figs. 2 and 3) attests the erosion/non deposition of a large part of the Sedrina Limestone formation in the AF's footwall. The contrast with the thick half-graben basin fill (Fig. 3) clearly indicates syn-sedimentary activity of the Amora Fault during the Early Jurassic. The Mt. Poieto reduced succession may represent the northern extension of the Mt. Cavallo paleo-high lacking the whole Lower Jurassic units (Rocca et al., 2024). The occurrence of disharmonic soft-sediment deformation slumps and coarse breccias in the Moltrasio Limestone along the Amora Fault further support this interpretation (Rocca et al., 2024, Figs. 4c, 5 and 6c). This is further supported by recent *in-situ* U-Pb dating of calcites from fault-related structures, which constrain the activity of normal faults of the Amora Fault System between Hettangian and Callovian (Table 1; Rocca et al., 2024). (2) The emplacement of an E-W trending swarm of andesitic dikes dating to the Eocene (Table 1; D'Adda et al., 2011), clearly crosscutting N-S-striking faults. These magmatic bodies were previously described by D'Adda et al. (2011) and Bergomi et al. (2015) as 4-5 m thick vertical andesitic dikes, associated to a small hypabyssal magmatic body intruded east of the Amora Fault System (Gandino area). The stock and the andesitic dike swarms have been dated around 40 Ma (U-Pb on zircons; Table 1; D'Adda et al., 2011). Apatite fission-track ages were indistinguishable from the zircon crystallization ages, suggesting a shallow emplacement depth of approximately 2-4 km (Table 1; Zanchetta et al., 2015). (3) N-S Alpine compression resulting in southward stacking of Dolomia Principale along the Albino Thrust. During this stage, most of the N-S-striking faults were reactivated as left-lateral strike-slip faults, consistently with a N-S directed compression. In the study area, the Albino Thrust extends about 6 km westward from the base of Mt. Rena, and it is covered by the Quaternary deposits of the Serio River to the east (Fig. 2). The NNW-SSE striking Nembro-Podona normal Fault with a right-lateral strike-slip kinematics (Fig. 2) produces complex geometries along the Albino Thrust, occurring along a facies transition between the Dolomia Principale inner platform and the Dolomie Zonate intraplatform basin (Berra and Jadoul, 1996). West of

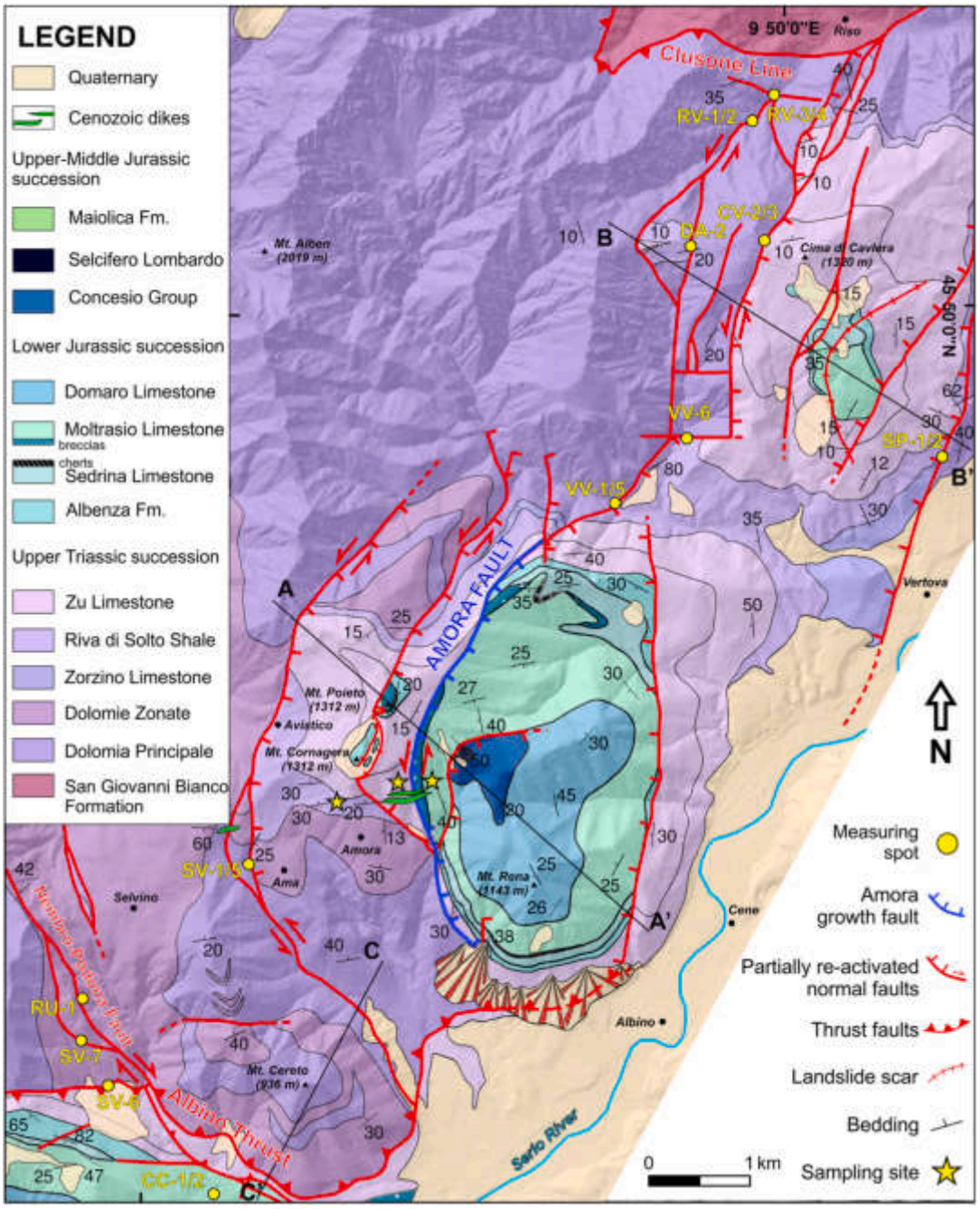

Fig. 2. Geological and structural map of the Seriana Valley area. Yellow stars indicate the position of samples. The name of the measuring spots is the same reported in figures displaying plots. Cross sections are displayed in Fig. 7 (AA'), 8 (BB') and 13 (CC'). (For interpretation of the references to colour in this figure legend, the reader is referred to the Web version of this article.)

the transverse zone, the thrust developed as a back-thrust, with the Dolomia Principale thrust sheet moving southward beneath the Upper Triassic succession (Zanchi et al., 1990), underthrusting the western area. In contrast, east of the right-lateral transverse zone, the Dolomia Principale is thrust southward on the Upper Triassic Zu Limestone and the folded Lower Jurassic succession forming duplexes between Nembro and Albino (Zanchi et al., 1990).

3. Methodology

Fieldwork was performed focusing on collecting orientation and kinematic data of brittle structures and analysing their crosscutting relationships. In the Seriana Valley area, a geological-structural map was produced at a 1:10,000 scale, integrated with a detailed one at a 1:2000 scale in the Amora area, with emphasis on secondary faults and fractures of the Amora Fault damage zone. The interpretation of the structural and stratigraphic setting of the study area was based on the revision of the available geological maps (Bersezio et al., 1997, 2012; Forcella and Jadoul, 2000; Jadoul et al., 2000, 2012) and on original detailed (m-scale) stratigraphic logs of the Lower Jurassic units in the footwall and hanging wall of the Amora Fault.

Approximately 600 deformation structures were measured at several sites, including beddings, mesoscopic fault planes, foliations, joints, slickenlines, veins, and tension gashes (see Tables S1 and S2 for measuring sites details). The different types of deformation structures are labelled as follows: V = vein, ST = tectonic stylolite, NF = normal

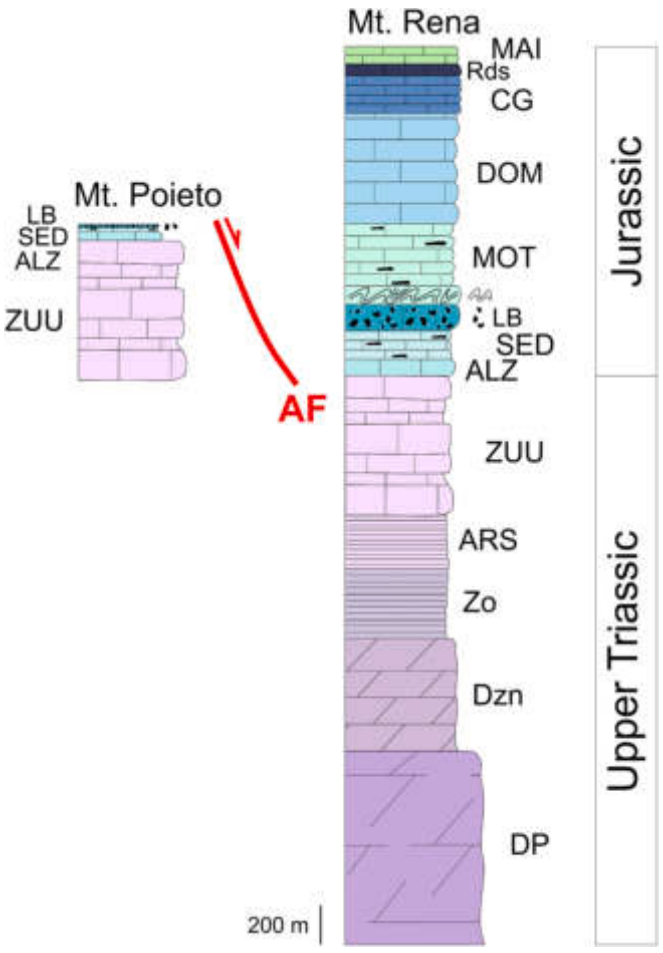

Fig. 3. Stratigraphic logs from Mt. Rena and Mt. Poieto showing variations in the thickness of the Lower Jurassic succession. AF - Amora Fault; DP -Dolomia Principale; Dzn – Dolomie zonate; Zo – Zorzino Limestone; ARS – Riva di Solto Shale, ZUU – Zu Limestone; ALZ – Albenza Formation; SED – Sedrina Limestone; LB – Lower Breccia of Moltrasio Limestone; MOT – Moltrasio Limestone; DOM – Domaro Limestone; CG – Concesio Group; Rds – Radiolariti del Selcifero Lombardo; MAI – Maiolica Formation.

fault, TF = thrust fault, SSF = strike-slip fault. Acronyms are systematically associated with a number indicating the tectonic phase. When more than one deformation structure of the same type occurs within the same tectonic phase, an additional letter is assigned based on crosscutting relationships. Additionally, veins and stylolites are assigned specific colour codes to aid in their visual identification.

Paleostress analyses were performed on selected fault populations according to their geometrical consistency and crosscutting relationships using the WinTensor software (Delvaux and Sperner, 2003). Internally consistent subsets of data out of the total and heterogeneous available dataset were identified. Then, a reduced paleostress tensor was derived for each tectonic phase, according to the following assumptions: (i) the stress tensor is homogeneous, (ii) strain is infinitesimal, and (iii) deformation is quasi-static (i.e., no relevant dynamic effects occur). These assumptions are usually met when (i) fault-slip data are collected at individual outcrops or in small homogeneous areas, and (ii) minor faults with limited offset are measured (this study). Initially, the fault slip data was tested using the "Right Dihedra method" (Angelier and Mechler, 1977) implemented in Wintensor (Delvaux and Sperner, 2003) to assess the internal consistency of the fault association and to obtain a general orientation of the stress tensor. Subsequently, the "Rotational Optimization" function was used to minimize normal stress and maximize shear stress for a selected fault population through an iterative approach (Delvaux and Sperner, 2003). The most consistent results were obtained for each fault surface by combining: (i) the misfit angle α between the observed slip vector and the computed maximum shear stress vector ("directional" contribution to the model), and (ii) the resolved normal to shear stresses ratio ("magnitude" contribution to the model). The inversion results were evaluated using the F5 function (F5 = 0 is a perfect fit, F5 = 360 is a perfect misfit), where values of F5 < 30° were considered acceptable for each solution. Additionally, it was ensured that α was <30° for each fault, following the common practice (Sperner and Zweigel, 2010) and our own experience in contractional domains (Zanchetta et al., 2023; Zanchi et al., 2006, 2021). Mainly striated fault planes were used, but in some cases, fault planes without slickensides were also included, as they are also reliable in constraining the stress tensor (Delvaux and Sperner, 2003). The quality of stress inversion solutions was evaluated with two indexes, QRWSM (Heidbach et al., 2018; Sperner et al., 2003) and QRT (Sperner et al., 2003). A summary of paleostress analyses is reported in Table 2.

24 deformation structures carrying carbonate phases were sampled exclusively along major fault zones, either directly from the main fault plane or within the damage zone and secondary faults (see Table S3 for details). The sampling criteria used in this study base on Roberts and Holdsworth (2022), who provide an empirical confidence scale for syn-kinematic carbonates. The collected samples include calcite slickenfibres, *en-échelon* tension gashes, and single-phase opening mode veins (Bons et al., 2012; Passchier and Trouw, 2005), from three key outcrops in the hanging wall and footwall of the Amora Fault. All structures can be attributed to distinct faulting events based on their orientation and crosscutting relationships.

Optical petrography was carried out on polished thin sections (n = 30) to detail crosscutting relationships between deformation structures, growth mechanisms of crystals (antitaxial, syntaxial, stretched) and their habitus (fibrous, blocky, elongated-blocky) based on the classification of Bons et al. (2012). Moreover, thin sections were etched and stained with a mixture of Alizarin red-S and potassium ferricyanide (Dickson, 1966) to recognise different carbonate phases (ferroan calcite, non-ferroan calcite, ferroan dolomite, non-ferroan dolomite). Cathodoluminescence microscopy was performed at the University of Milano-Bicocca, using a cold RELIOTRON CONTROL mounted on a Nikon ECLIPSE LV100ND POL optical microscope. Cathodoluminescence (CL) observation were conducted under a vacuum of 60-50 mTor at 6-7 kV and 1.2-1.4 mA. The same settings were maintained for all image acquisitions. CL microscopy was useful to assess the occurrence of several carbonate phases, based on their luminescence response (non-luminescent, dull-red, bright red), and to evaluate the homogeneity of each carbonate phase to rule out possible subsequent alteration events (see Fig. S1 in Supplementary material).

4. Structural and paleostress analyses of the Amora Fault System

Starting from the general reconstruction of the evolution of the Amora Fault System provided by Zanchi et al. (1990), we performed new detailed field structural analyses in the whole area. Structural and paleostress analysis data are presented according to the recognized three main deformational events. For each stage, carbonate-bearing structures are described. Veins, stylolites, and secondary faults are grouped based on their relative chronology and crosscutting relationships. These structures are characterized by the presence of several carbonate phases, which are briefly described below.

4.1. *N-S-striking normal faults*

The Amora Fault System is primarily characterized by NNE-SSW-striking normal faults that dissect the Upper Triassic carbonate succession and accommodate displacements of several hundred meters (Fig. 2). The key structure is the Amora Fault, a N-S-striking, 4 km-long normal fault (Fig. 2). It separates a 1 km-thick Rhaetian to Hettangian

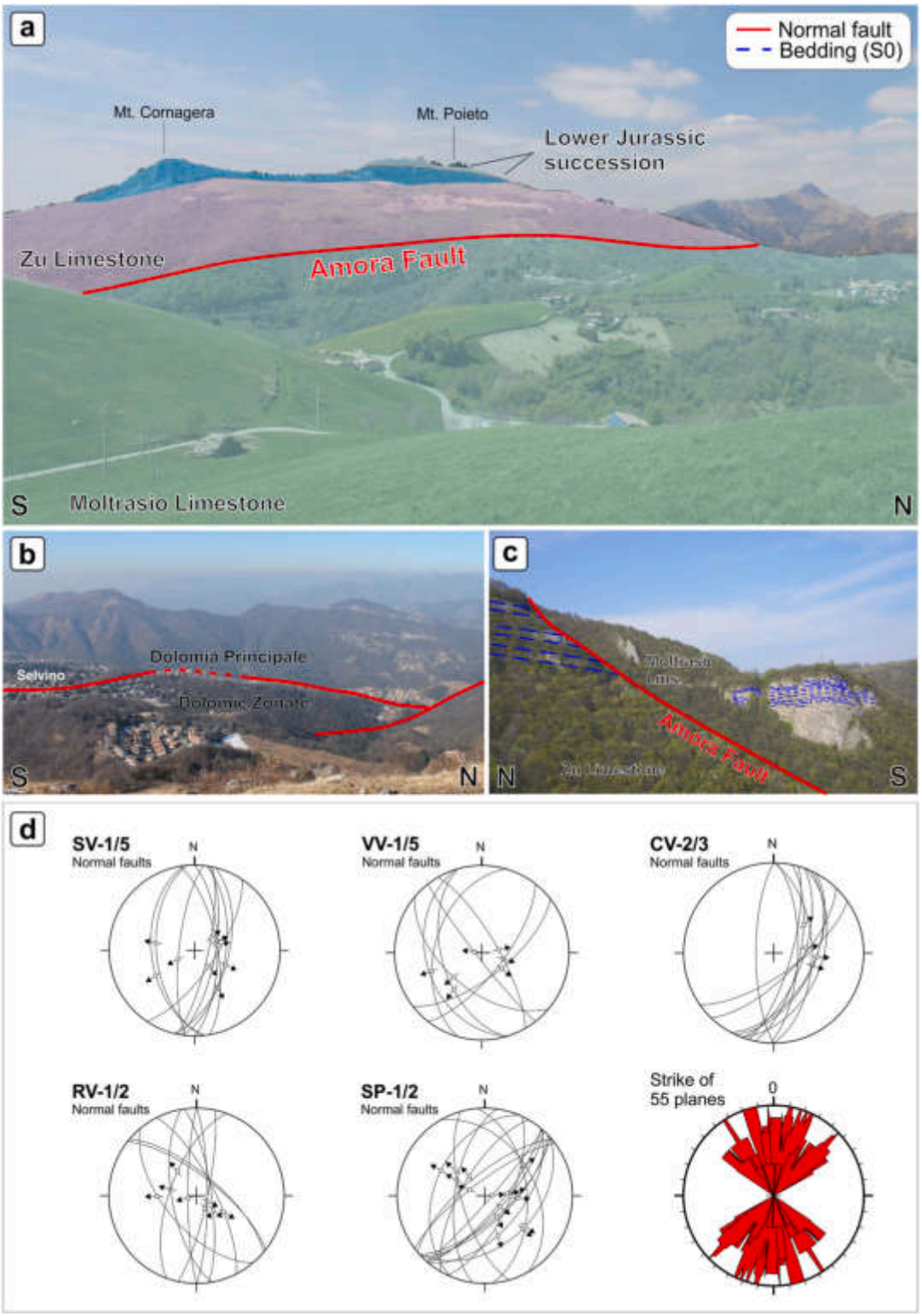

Fig. 4. **(a)** Panoramic view of the eastern Mt. Poieto–Mt. Cornagera sector. The Amora Fault juxtaposes Rhaetian Zu Limestone (footwall) against Sinemurian Moltrasio Limestone (hanging wall). The Lower Jurassic succession is reduced on the Mt. Poieto paleo-high relative to the Mt. Rena half-graben. **(b)** N–S-trending normal fault at the facies boundary between the Norian Dolomia Principale and Dolomie Zonate, near Selvino. **(c)** Panoramic view of the Amora Fault along the road-cut between Amora and Ganda. **(d)** Structural data of normal fault planes measured in key sites in the Seriana Valley area. The location of the measuring spots is reported in Fig. 2. Rose diagram of the strike of normal fault planes is also reported.

succession (the Mt. Poieto paleo-high) in the hanging wall, from a 2.8 km-thick Rhaetian to Lower Cretaceous succession (the Mt. Rena half-graben) in its footwall. The Lower Jurassic Moltrasio Limestone in the hanging wall is juxtaposed to the Upper Triassic Zu Limestone in the footwall with a stratigraphic separation of 600 m (Figs. 2–4). The AF dips steeply to the east and exhibits normal dip-slip movements (Figs. 4 and 5).

The main fault plane extends northward to the west of Mt. Cavlera,

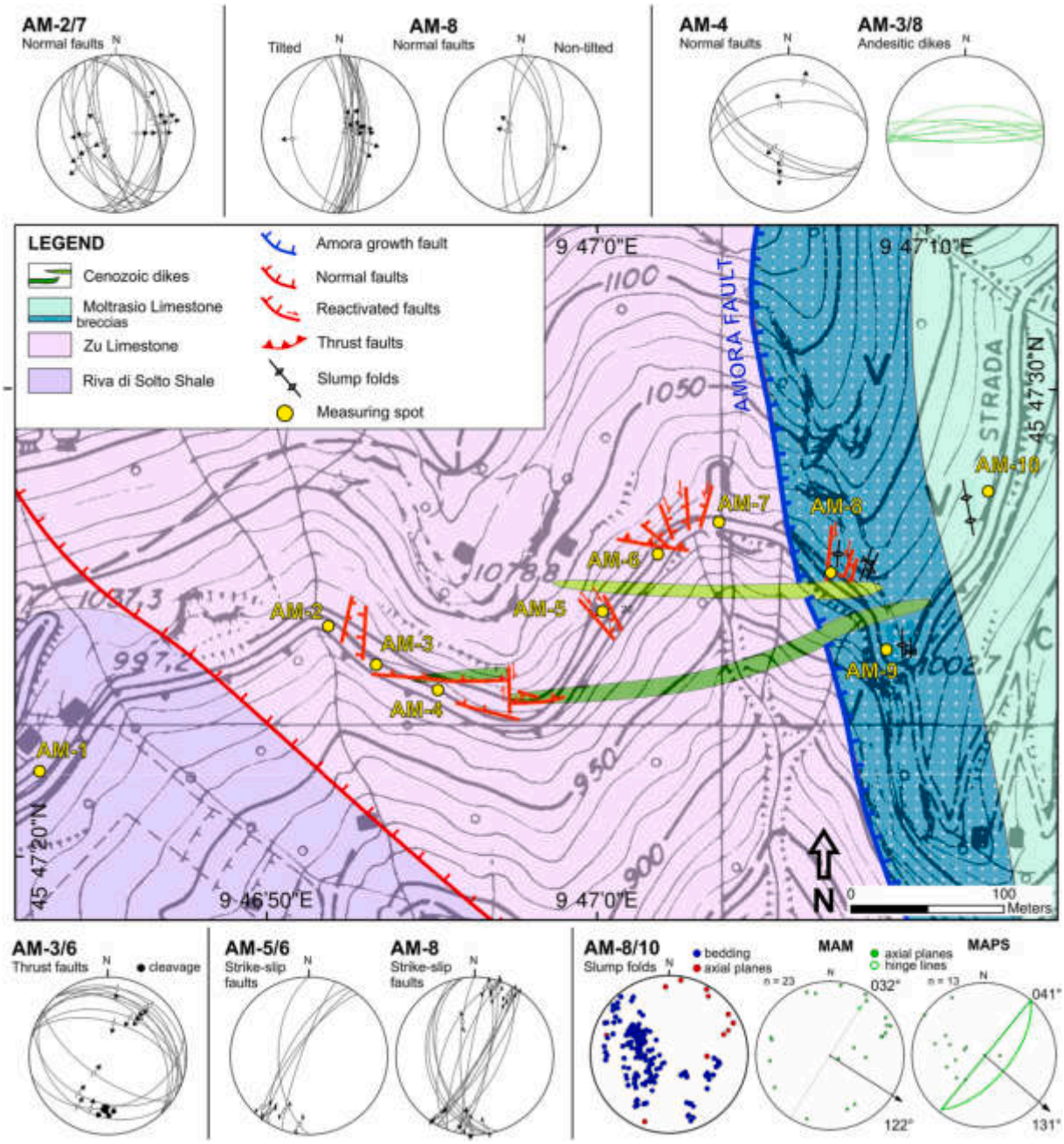

Fig. 5. Geological and structural map of the Amora area with structural data from key sites. AM-1: Riva di Solto Shale; AM-2–7: Zu Limestone (footwall of AF); AM-8–10: Moltrasio Limestone (hanging wall of AF). AM-8–10 include statistical analyses of slump folds (MAM and MAPS methods; Alsop and Marco, 2012). Arrow shows sediment transport direction along the paleo-slope.

where it juxtaposes the Norian Dolomia Principale and the Rhaetian Zu Limestone, dipping to the East. South of Mt. Cavlera, the fault is displaced 1 km to the East by an E-W-striking left-lateral strike-slip fault (Fig. 2). The fault then splays into several NNE-SSW-striking branches that cut through the Norian succession and are crosscut by the Clusone Fault or intersect with E-W-striking faults (Fig. 2). North-West of Mt. Cavlera, near the main fault plane, several N-S-striking conjugate faults with medium to high-angle dip-slip normal striations were measured (CV-2/3; Figs. 2 and 4d). Similarly, in the Riso Valley, conjugate fault planes striking NNW-SSE to N-S also display high-angle dip-slip normal kinematics (RV-2/3; Figs. 2 and 4d).

West of the Mt. Poieto paleo-high, another fault displaces the Upper Triassic succession. Its northern segment trends NNE-SSW, parallel to the Amora Fault, and primarily displays a normal displacement, while its southern segment bends towards NNW-SSE, exhibiting left-lateral strike-slip motions (Fig. 2). Normal faulting was confirmed by the occurrence of several N-S-striking, high-angle conjugate fault planes with dip-slip striations (SV-1/5; Figs. 2 and 4d). The Amora Fault appears to extend further north, where it takes on a NNE-SSW trend, cutting through the Norian succession, where it is offset by N-S-striking normal fault segments (Fig. 2). Herein, two sets of conjugated fault planes striking NNW-SSE and dip-directions towards NE and SW, with intermediate to high dip angles and dip-slip normal movements have been documented (VV-1/5; Figs. 2 and 4d).

In the northeastern part of the study area, a NNE-SSW fault borders Mt. Cavlera, dipping to the W and juxtaposing the Norian succession (Dolomia Principale, Dolomie Zonate and Riva di Solto Shale) to the Rhaetian Zu Limestone (Fig. 2). Herein, NNE-SSW conjugate fault planes

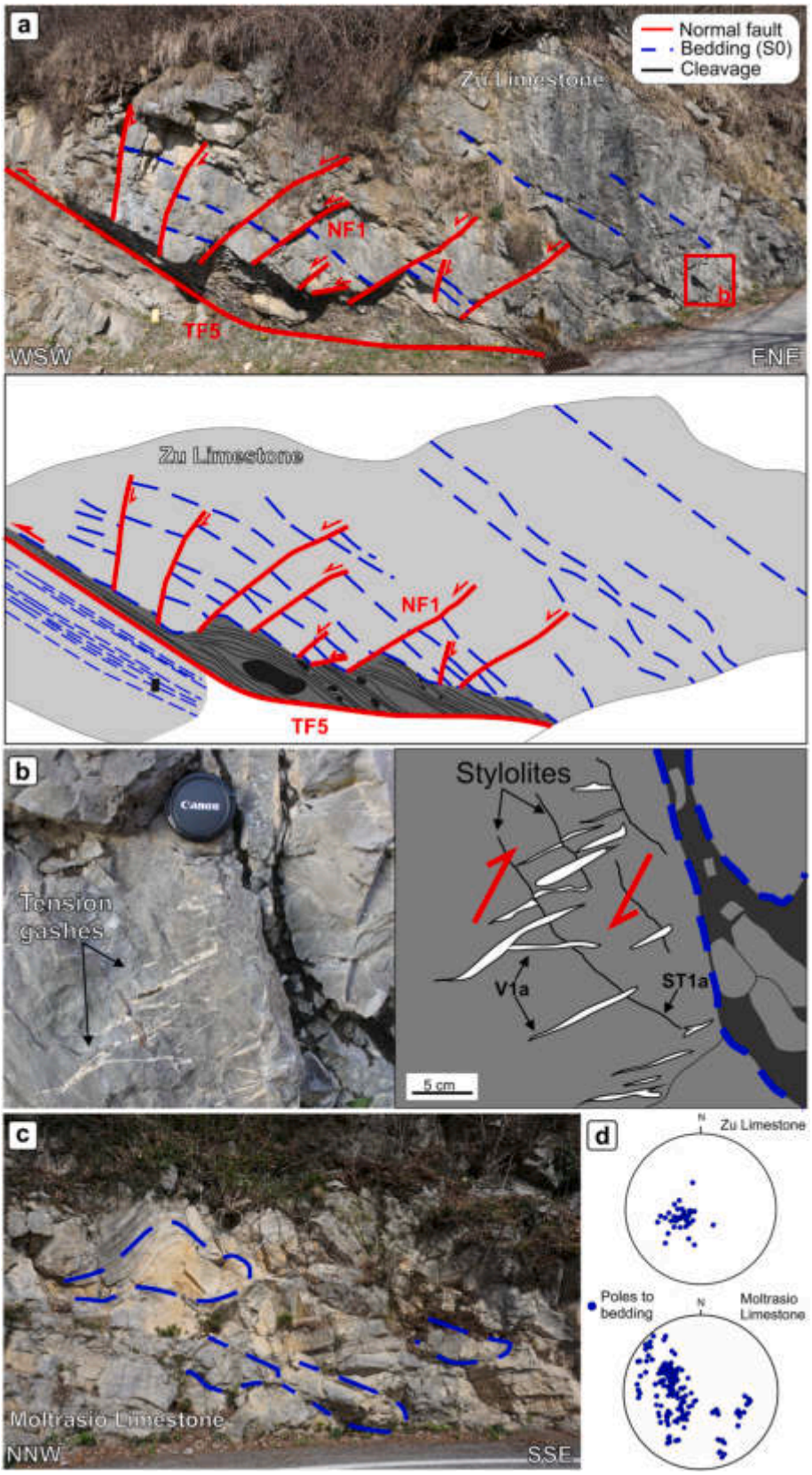

Fig. 6. Mesoscale structural analysis of Amora area **(a)** Mesoscopic blocks displaced by domino-style normal faults (NF1) forming Andersonian horst and graben structures, tilted by a secondary thrust fault (TF5) within the Zu Limestone (footwall of AF). **(b)** *En-échelon* tension gashes in Zu Limestone. NF1, V1a and ST1a refer to fracture sets, as reported in Fig. 9. **(c)** Slump folds in the Moltrasio Limestone (footwall of AF). **(d)** Stereographic projections (equal area, lower hemisphere) of poles to the bedding planes measured in the hanging wall and footwall of the AF.

Table 1
Summary of geochronological constraints for the Seriana Valley area. Sample type, structure, location, and dating technique are reported. Age data are reported with 2σ uncertainties, together with the corresponding references. Deformational events are reported according to this study and as shown in the figures.

Sampled Structure	Location	Mineral type	Age ± 2σ (Ma)	Method	Deformative event	Reference
Stylolites, Slickenfibres, Tension gashes	Amora area (AM-7, Fig. 5)	calcite	**192.4 ± 8.4 - 164.4 ± 8.6**	*in-situ* LA-ICP-MS U-Pb dating	(1) E-W extension	Rocca et al. (2024)
Andesitic dikes	Amora and Gandino areas	zircon	**39.0 ± 1.0**	SHRIMP U-Th-Pb dating	(2) N-S extension	D'Adda et al. (2011) Bergomi et al. (2015)
Andesitic dikes	Amora area	apatite	**37.0 ± 6.1**	Apatite Fission Track dating	Post-dike emplacement	Zanchetta et al. (2015)

Table 2
Summary of paleostress analyses performed with Wintensor. ID indicates the name of the measuring site as reported in Figs. 2 and 14. The total number of measures and the number of accepted faults for stress inversion are indicated as "Data" and "Used", respectively. Trend and plunge of σ_1, σ_2 and σ_3 are reported along with 1 sigma standard deviation ($\sigma_1 \geq \sigma_2 \geq \sigma_3$). R is the stress ratio as $R = (\sigma_2-\sigma_3)/(\sigma_1-\sigma_3)$, and R' is the tectonic stress regime index, $R' = R$ when σ_1 is vertical (extensional stress regime), $R' = 2- R$, when σ_2 is vertical (strike-slip stress regime), $R' = 2+R$, when σ_3 is vertical (compressional stress regime). α is the angle between the slip vector on the fault plane and the computed shear stress with standard deviation (solutions accepted for $\alpha < 30°$). The Misfit function F5 ranges between 0 and 360 from perfect fit to complete misfit (solutions accepted for F5 < 30). QR_{WSM} and QR_T are quality estimator indexes from Delvaux and Sperner (2003), both ranging from A (best quality) to E (worst quality).

ID	Data	Used	σ_1			σ_2			σ_3		
			Trend	Plunge	1σ	Trend	Plunge	1σ	Trend	Plunge	1σ
SV-1/5	11	10	247	81	17	1	4	35	91	8	34
RV-1/2	11	10	36	85	4	193	5	4	283	2	1
VV-1/5	10	8	164	80	16	323	9	16	53	4	4
CV-2/3	18	11	16	85	26	181	5	32	272	1	35
SP-1/2	18	16	13	88	18	219	2	19	129	1	11
RV-3/4	11	4	213	81	18	93	5	18	3	8	10
SV-6	17	9	347	3	18	77	1	12	180	87	14
CC-1/2	25	25	8	2	40	98	2	40	227	87	10
RU-1	20	20	189	1	13	281	69	35	99	21	35
SV-1/5	11	11	187	7	18	36	82	18	277	4	16
SV-7	20	16	174	0	12	83	70	16	264	20	12
AM-2/7	15	15	33	82	16.9	167	6	15.9	257	6	14.9
AM-8	15	15	279	62	20.1	182	4	13.4	90	28	19.9
AM-8	7	7	161	85	20.8	2	5	17.4	272	2	16.5
AM-4	6	6	17	86	20	277	1	31	187	4	32
AM-3/6	12	12	35	6	16	125	1	12	223	84	14
AM-5/6	5	5	166	26	19	316	61	18	70	13	19
AM-8	17	16	180	10	7.5	279	42	8.7	80	46	4.8

Ratio R	Ratio R′	St-dev	α	St-dev	F5	St-dev	QRwsm	QRt
0.1	0.1	0.13	11	7.9	4.9	5.7	C	C
0.16	0.16	0.1	8.7	5.3	2.8	2.3	D	D
0.24	0.24	0.14	4.4	3.3	1.5	1.1	D	D
0.28	0.28	0.19	2.9	6.1	1.2	2.8	C	D
0.24	0.24	0.15	8.8	7.7	3.8	4.4	B	B
0.18	0.18	0.14	4.8	2.8	0.8	0.8	E	E
0.73	2.73	0.29	5.9	7.1	2.2	4.1	D	D
0.94	2.94	0.31	7	7.8	5.4	6.1	A	A
0.03	1.97	0.1	16	9.8	8.8	8.1	D	D
0.37	1.63	0.32	9.7	5.7	3.4	2.8	C	C
0.12	1.88	0.17	14	9.2	7.6	6.8	C	C
0.43	0.5	0.15	10.4	6.8	4.4	4.7	C	C
0.5	0.5	0.28	5.4	6.4	2.4	3.1	B	D
0.5	0.5	0.17	5.4	6.4	1.6	2.3	D	D
0.07	0.07	0.1	7.2	3	2	1.7	D	D
0.6	2.6	0.37	4.2	3.7	1.7	2.6	C	C
0.18	1.02	3.5	4.1	2.3	1.2	0.5	E	E
0.12	2.12	0.08	11.9	9.8	6.2	7.8	B	C

dipping at high angle towards SE and NW have been measured in the Dolomie Zonate showing dip-slip normal movements (SP-1/2; Figs. 2 and 4d). Similarly, the eastern side of Mt. Rena is bounded by a N-S-striking W-dipping antithetic normal fault, juxtaposing the Zu Limestone in the footwall to the Moltrasio Limestone in the hanging wall (Fig. 2).

In the Amora area, the Zu Limestone is affected by the damage zone of the AF. Here, mesoscopic tilted blocks are displaced by domino-style N-S-striking normal faults and Andersonian horst and graben structures (Figs. 5 and 6a). Centimetre to meter normal displacements is indicated by offset beds of the Zu Limestone. Carbonate slickenfibres suggest dip-slip normal movements along high-angle fault planes (AM-2/7; Figs. 5 and 6a).

In the hanging wall of the Amora Fault, two distinct fault populations were identified within the Moltrasio Limestone: (1) N-S-striking tilted normal faults in conjugate sets, dipping at high angles, which are crosscut by (2) N-S-striking post-tilting normal faults, also in conjugate sets with high-angle dips (Figs. 5 and 6a). Both fault populations exhibit dip-slip slickenfibres, indicating normal movements (AM-8; Fig. 5).

Paleostress tensors obtained for the N-S-striking normal fault populations measured at stops SV-1/5, RV-1/2 and CV-2/3 show a vertical

σ1 and a sub-horizontal NNW-SSE σ3 (Figs. 7 and 8). At stops VV-1/5 and SP-1/2 σ3 trend NE-SW and NW-SE, respectively (Fig. 8). The paleostress solutions in both cases suggest an E-W oriented σ3 for the first tectonic stage recognizable for the Amora Fault System (Figs. 7b and 8b). The solutions obtained for N-S-striking normal fault populations in the Amora area align with those above described. The data show a vertical σ1 and an NNE-SSW (AM-2/7; Fig. 7b) to E-W σ3 (AM-8; both tilted and non-tilted faults; Fig. 7b).

Several carbonate-bearing structures are associated with this stage (Fig. 6b), and their relative chronology is summarized in Fig. 9. Number "1" corresponds to the Early-Middle Jurassic tectonic stage, while number "2" represents the Late Jurassic–Early Cretaceous final stages of rifting. Additionally, because multiple generations of tension gashes formed during Early Jurassic rifting (V1 in Fig. 9), each set has been assigned a letter and colour code to indicate its relative age based on crosscutting relationships ("a" denotes the oldest set, and "d" the youngest; Fig. 9).

V1a is characterized by strata-bound bed-normal tension gashes occurring in the Zu Limestone, typically organized in NNE-SSW trending *en-échelon* arrays. These are associated to WNW-ESE trending tectonic stylolites (ST1a), slightly oblique (~10°) to the bedding (Figs. 6b and 9). V1a and ST1a are crosscut by NE-SW trending S-shaped tension gashes (V1b), arranged in *en-échelon* arrays giving a top-to-SW shear sense (Fig. 9). V1c is represented by NNW-SSE trending bed-normal tension gashes in Zu Limestone, crosscutting V1b (Fig. 9). V1c sets are then crosscut by N-S-trending V2 opening mode-I veins (Bons et al., 2012, Fig. 9) that preferentially occur in the Riva di Solto Shale, cutting through both carbonates and shales layers. In the footwall of the Amora Fault, V1a, ST1a, V1b, and NF1a were rotated along with bedding during rifting in zones close to the main fault plane (AM-6/7; Figs. 5 and 6a), whereas bedding becomes almost horizontal moving away from the fault zone (AM-1/5; Fig. 5). These deformation structures are filled up with multiple carbonate phases. V1a, ST1a, V1c, and NF1a contain blocky to elongated-blocky calcite exhibiting dull-red luminescence. V1b, V1c, and NF1b are filled with saddle dolomite, showing evidence of partial to complete dedolomitization, and are non-luminescent. Finally, the V2 extension veins display syntaxial fibrous calcite crystals with dull-red luminescence (see Fig. S1).

4.2. *E-W trending andesitic dikes and normal faults*

E-W trending dikes crosscut the N-S-striking normal faults of the Amora Fault System, particularly in the Amora and Selvino areas.

E-W-striking faults parallel to the dikes displace the N-S-striking

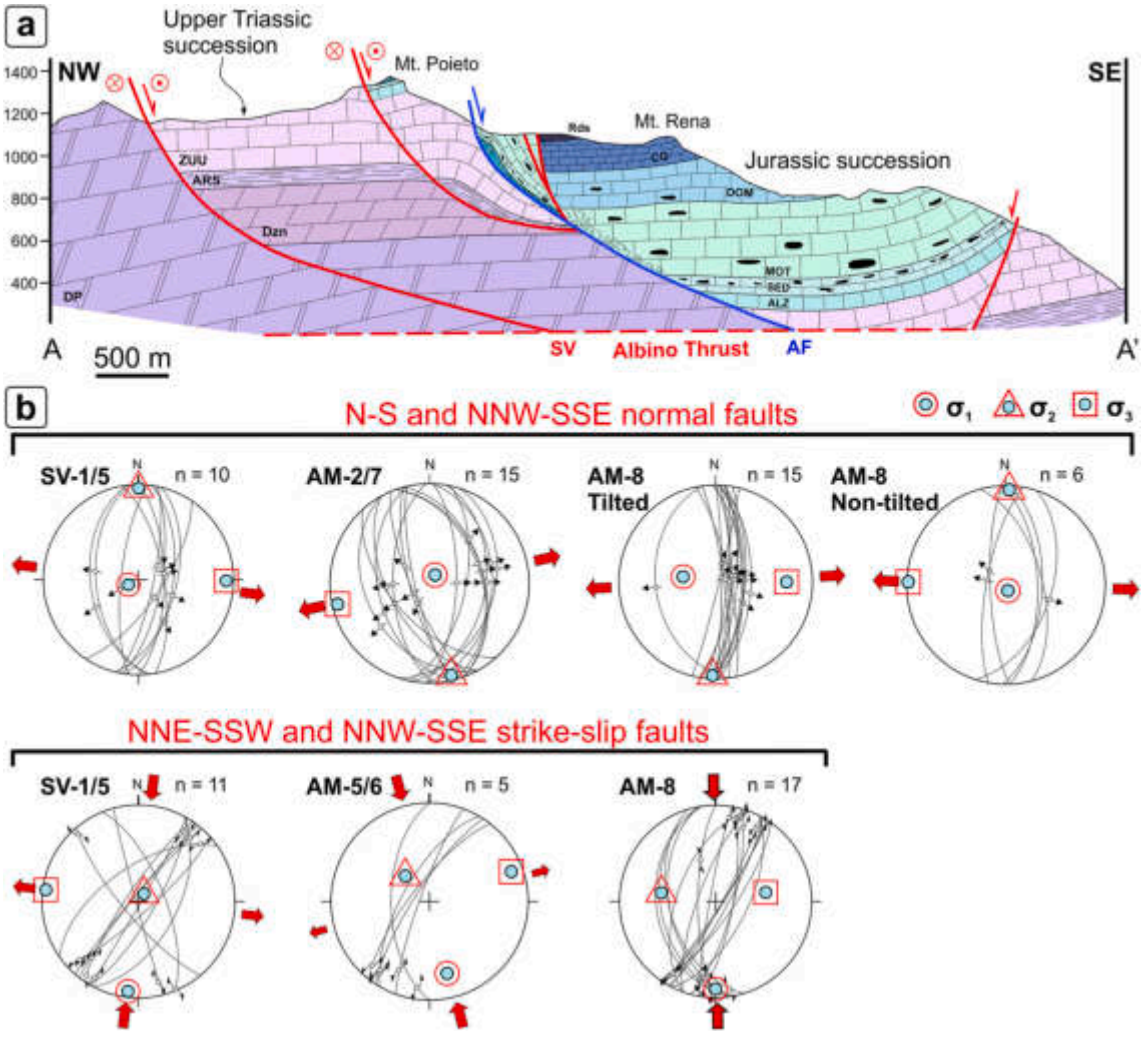

Fig. 7. **(a)** Schematic cross section across the Mt. Poieto – Mt. Rena area. The Mt. Rena half-graben displays a thicker Jurassic succession compared to the Mt. Poieto paleo high. AF – Amora Fault. **(b)** Fault planes from Selvino (SV-1/5) and Amora (AM-2/8) show normal kinematics consistent with E–W extension, with evidence of strike-slip reactivation due to N–S Alpine compression. Measurement sites are indicated in Fig. 2 and 14. DP -Dolomia Principale; Dzn – Dolomie zonate; ARS – Riva di Solto Shale, ZUU – Zu Limestone; ALZ – Albenza Formation; SED – Sedrina Limestone; LB – Lower Breccia of Moltrasio Limestone; MOT – Moltrasio Limestone; DOM – Domaro Limestone; CG – Concesio Group; Rds – Radiolariti del Selcifero Lombardo.

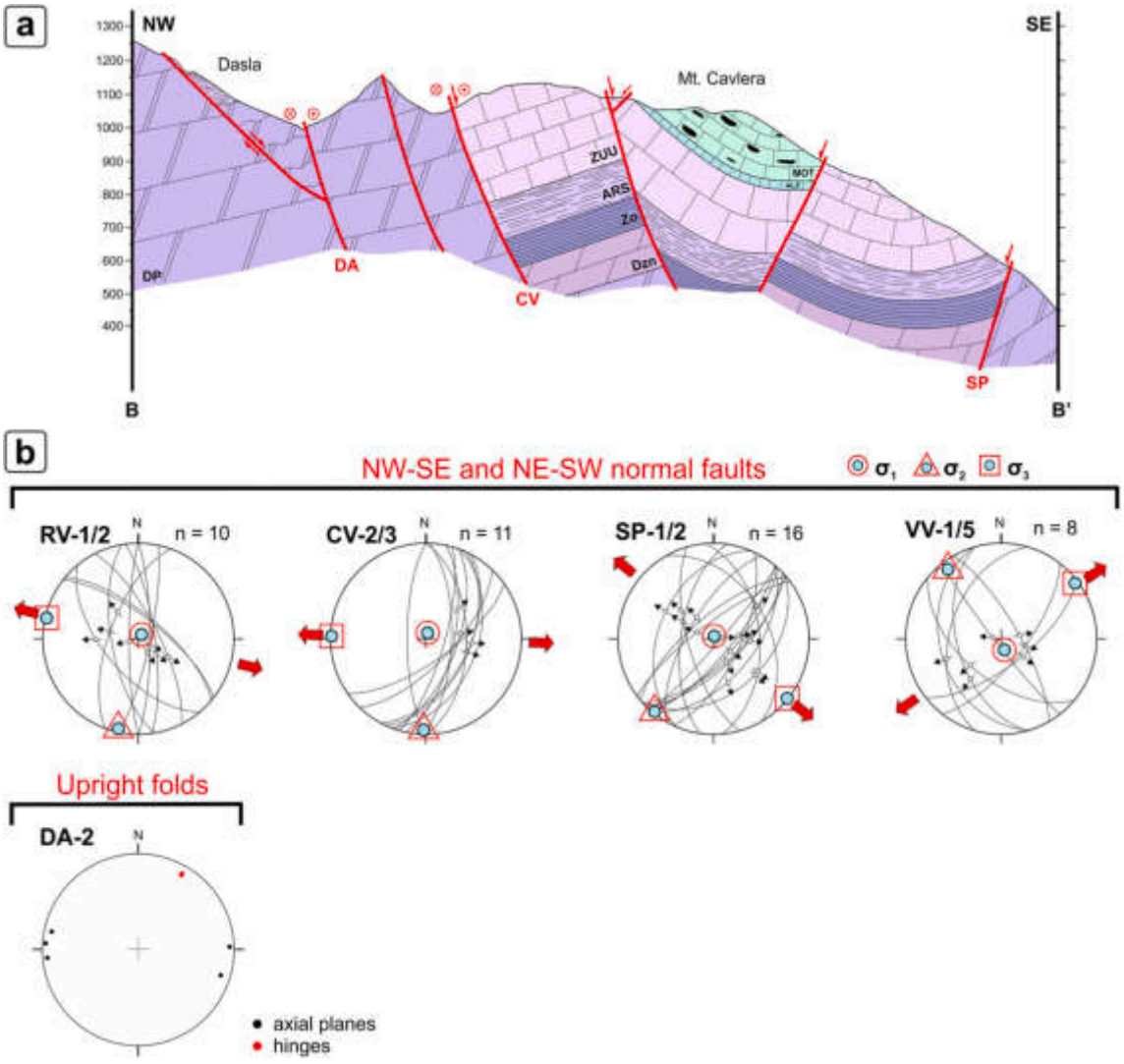

Fig. 8. **(a)** Schematic cross section of the Mt. Cavlera area. In the Dasla area (DA), strike-slip reactivation of rift-related normal faults folds the Upper Triassic succession, forming a positive flower structure. **(b)** Normal faults in the Seriana Valley indicate E–W extension. Fault sets at VV-1/5 and SP-1/2 show clockwise and counterclockwise σ_3-axis rotation, respectively. Axial planes and fold hinges in the Dasla area reflect strike-slip reactivation of pre-existing faults. DP -Dolomia Principale; Dzn – Dolomie zonate; Zo – Zorzino Limestone; ARS – Riva di Solto Shale, ZUU – Zu Limestone; ALZ – Albenza Formation; MOT – Moltrasio Limestone.

normal fault system (Figs. 2 and 10). Conjugate E-W faults and joints were measured in several localities, and at the RV-3/4 (Riso Valley) high-angle planes show growth fibres and steps, confirming dip-slip normal movements (Fig. 10). Similarly, in the footwall of the Amora Fault, E-W-striking conjugate faults (NF4 in Fig. 9) offset the andesitic dikes (Fig. 11a). Slickenfibres and growth steps indicate dip-slip normal kinematics (AM-3/4; Fig. 10) as in the Presolana area to the north (D'Adda et al., 2011).

E-W-striking normal fault populations measured in the Riso Valley (RV-3/4, Figs. 2 and 10) display enough fault planes with well-preserved kinematic indicators to apply paleostress analysis. The obtained solutions indicate a vertical σ_1 and a N-S trending σ_3 (Fig. 10). In the Amora area, several conjugate fault planes were measured, yielding a sub-horizontal NNE-SSW σ_3 (AM-6/7; Figs. 5 and 10). Obtained paleostress solutions are consistent with the ones obtained by D'Adda et al. (2011) in the Gandino area.

4.3. Alpine structures: thrusts and strike-slip reactivations

The Albino Thrust is the major structure related to the Alpine compression in the lower Seriana Valley. Along this fault, the Upper Triassic succession is thrust southward on the uppermost Triassic and Jurassic units (Fig. 2).

Mesoscale conjugate thrust faults were identified in the Dolomia Principale east of the transverse zone (SV-6; Figs. 2 and 12d). These E–W-striking, N- and S-dipping low-angle planes display slickenfibres indicating reverse dip-slip movements. Similar structures, together with a prominent train of south-verging fault-propagation folds, occur in the Lower Jurassic succession at Cava Cugini (Nembro village; Fig. 12b and d). Here, NNW–SSE-striking secondary thrusts show reverse kinematics along medium-to low-angle planes (CC-1/2; Fig. 12b–d and 13). The area is dominated by a south-verging recumbent fold with an E–W-trending hinge and N-dipping axial planes (Fig. 12b–d and 13). In the well-bedded Lower Jurassic units, south-verging open to tight parasitic folds with E–W trending hinges and associated axial-plane cleavage are accompanied by flexural-slip planes showing dip-slip movements (CC-1/2; Figs. 12d and 13).

Other measuring sites located along the strike-slip Nembro-Podona fault zone mainly show NNW-SSE right-lateral motions. In the damage zone extending laterally up to 200 m, several NNW-SSE right-lateral and NNE-SSW left-lateral conjugate fault planes were measured, showing sub-horizontal slickenfibres and growth steps (RU-1 and SV-7; Figs. 12d

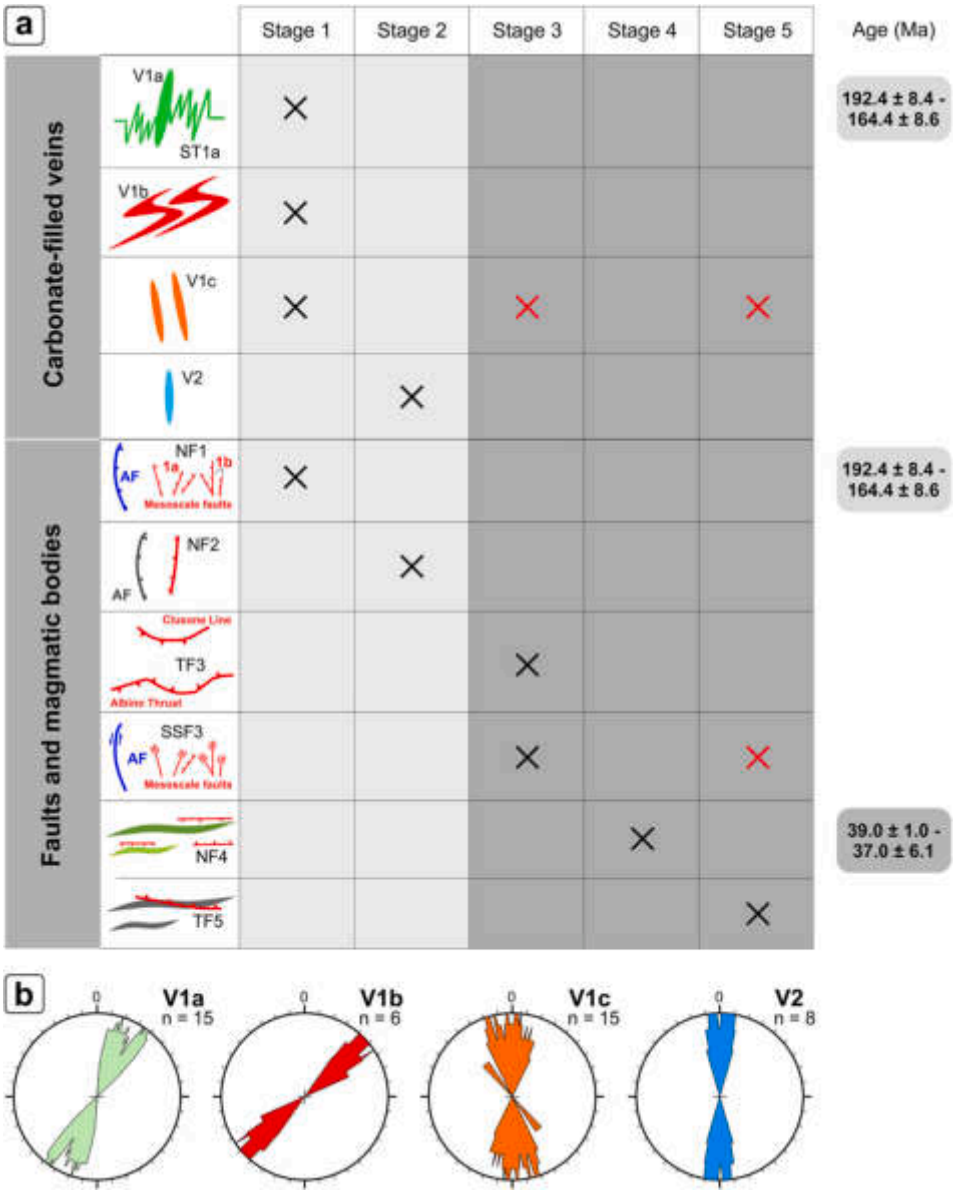

Fig. 9. **(a)** Cross-table of tectonic structures and corresponding tectonic stages. Black crosses refer to the formation of the structures, whereas red crosses refer to the re-opening of veins or reactivation of faults in a subsequent tectonic stage. Stage 1 and 2 relate to Jurassic rifting event (light background), Stage 3-5 are Alpine compression events (darker background). Letters (a–d) mark mesoscale cross cutting relationships between mineralised fractures. V – tension gashes or extension vein; ST – stylolite; NF – normal fault; TF – thrust fault; SSF – strike-slip fault. Geochronological data are reported according to Table 1. **(b)** Rose diagrams showing the N-S to NE-SW trend of tension gashes and veins, consistent with the Jurassic rifting events. (For interpretation of the references to colour in this figure legend, the reader is referred to the Web version of this article.)

and 13). West of Mt. Poieto paleo-high, along the previously described left-lateral strike-slip structure, NNE-SSW and NNW-SSE high-angle conjugate strike-slip faults occur, crosscutting previous N-S-striking normal faults. The sense of movement was identified by sub horizontal striations with growth steps, Riedel R and stylolites (SV-1/5; Fig. 12d).

The NNE-SSW faults bordering the western side of Mt. Cavlera displays a left-lateral motion. Herein, in the Norian Dolomia Principale a positive-flower structure was observed (Figs. 12a and 13a). In this area, the Norian-Rhaetian succession filling the small graben is deformed by a series of upright folds with N-S-trending hinges steeply dipping to the E and W (DA-2; Figs. 12a and 13). These are offset (about 1 m) by N-S-striking reverse faults (Fig. 12a).

In the Amora area, N-S conjugate normal faults were reactivated as left- or right-lateral strike-slip faults, both in the footwall and hanging wall of the AF (AM-6/8; Figs. 5 and 11d). Their kinematics was reconstructed from slickenfibres with carbonate growth steps crosscutting earlier dip-slip indicators (Fig. 11d). Additionally, a horizontal NW-SE-striking, N-dipping thrust fault clearly displaces an andesitic dike (AM-3; Figs. 5 and 11a, b). Several conjugate NW-SE-striking thrust planes were measured, with low to moderate angles (AM-3, AM-5/6; Fig. 5). In a shale-rich layer of the Zu Limestone, a north-dipping high-angle cleavage occurs, consistent with thrusting (Figs. 5 and 11a, c).

Paleostress solutions for thrust faults measured in the hanging wall of the Albino Thrust (SV-6; Fig. 13b) display a sub-horizontal NNW-SSE σ1 and vertical σ3. Similarly, for the footwall (CC-1/2; Fig. 13b) the inversion shows a sub-horizontal NNE-SSW σ1. Paleostress tensors obtained for the strike-slip conjugate systems at stops RU-1 and SV-1/5 result in an NNE-SSW σ1, while at stop SV-7 a N-S σ1, and vertical σ2 are observed (Fig. 13b). The results for the Amora area are consistent, showing a NNE-SSW σ1 and vertical σ3 for thrust faults measured in the

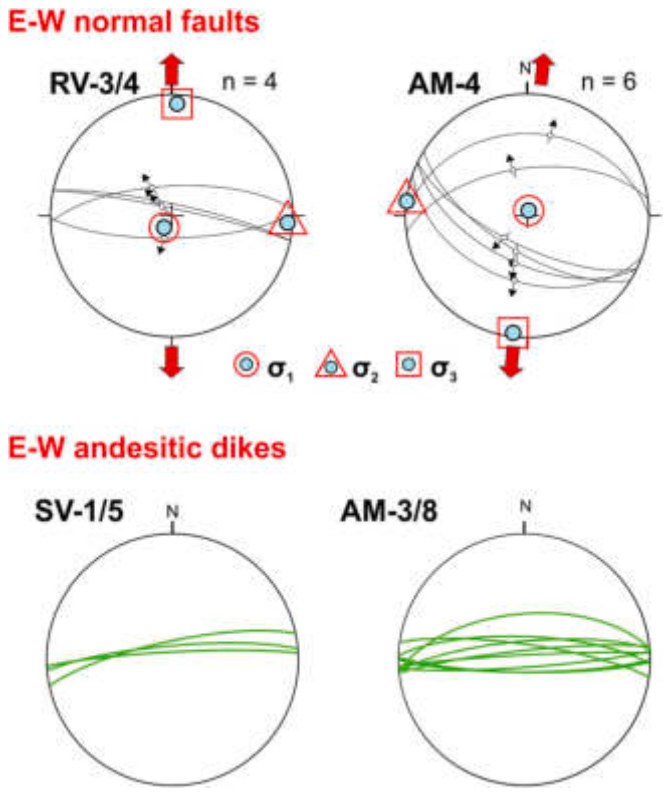

Fig. 10. Fault-slip measurements on normal faults and orientations of andesitic dikes formed during the mid-Eocene N–S extensional event.

footwall of the AF (AM-3/6; Fig. 13b), and a NNW-SSE to N-S σ1 and vertical σ2 for strike-slip faults (AM-6/8; Fig. 7b). These data suggest a general N-S oriented compression. Principal stress axes orientation is also consistent with the shortening direction suggested by orientation of measured folds (CC-1/2 and DA-2 in Fig. 12) and cleavages (CC-1/2 and AM-5, Fig. 13b).

Carbonate strike-slip slickenfibres on reactivated N–S-striking fault planes occur in the Moltrasio Limestone as well (SSF3; Figs. 9 and 11d). They are characterized by blocky calcite crystals showing dull-red luminescence (see Fig. S1). During the Alpine compression stages, V1c tension gashes were reopened and filled with a fine-grained blocky calcite cement, displaying dull-red luminescence (see Fig. S1).

5. Discussion

5.1. The polyphase tectonic evolution of the Amora Fault System

5.1.1. Jurassic extension

Crosscutting relationships confirm a multi-stage tectonic evolution of the Amora Fault System. The first stage is characterized by N-S-striking normal faults formed in response to the Jurassic rifting event (Rocca et al., 2024). Stratigraphic and sedimentological evidence (i.e., the thick half-graben basin fills vs the reduced paleo-high succession, and soft-sediment deformation slumps) indicate that the Amora Fault System was active during the late Hettangian-Sinemurian, simultaneously with the deposition of the Moltrasio Limestone (Zanchi et al., 1990). Field-based observation of wedge-shaped deposits and slump folds statistical analysis in the hanging wall of the Amora Fault (Rocca et al., 2024), along with paleostress analysis (Fig. 14), all point out that the Amora Fault System accommodated E-W rift-related extension in the Early Jurassic (Fig. 15a). Moreover, the Toarcian-Bathonian Concesio Group, more than 100 m thick in the Mt. Rena half-graben but totally missing west of the Mt. Poieto-Nese high, is replaced by the Sogno Formation to the west (Fig. 1b; Casati and Gaetani, 1968; Mattioli and Erba, 1999; Rocca et al., 2024). The Amora Fault was hence active during the Middle Jurassic separating the Mt. Rena half-graben basin to the east, from the Ubiale Basin to the west (Fig. 1b; Rocca et al., 2024). Recent *in*-situ U-Pb ages suggest that the Amora Fault System was active throughout the Jurassic, with intermittent pulses of activity lasting several million years (192.4 ± 1.7|8.4 – 169.4 ± 4.6|8.6 Ma on V1a, ST1a and NF1a tectonic sets; Rocca et al., 2024). In the Amora Fault damage zone, fractures aligned with the E-W oriented extension were sealed by various carbonate cements that allow to further identify two sub-stages: 1a and 1b (Fig. 15a). During stage 1a (Hettangian – Bajocian; Rocca et al., 2024), secondary normal faults (NF1a), stylolites (ST1a), and tension gashes (V1a) formed in the footwall of the AF (Fig. 9). Calcite cement precipitated along NF1a fault planes, sealing ST1a and V1a fractures. In stage 1b (Bajocian – Callovian?), renewed post-rift activity was accompanied by the formation of new fractures, including V1b and V1c tension gashes and NF1b secondary normal faults. These fractures were sealed by diverse carbonate cements.

In the footwall of the AF N-S-trending extension veins (V2) have been observed crosscutting previous tectonic sets (Fig. 9). These can be related to a reactivation (Stage 2) at the end of the Late Jurassic. Previous studies (Bersezio et al., 1993; Castellarin, 1972; Winterer and Bosellini, 1981) reported a reprisal of syn-sedimentary activity along the Ballino-Garda fault system from the Tithonian to the Lower Aptian, during the deposition of the Maiolica Formation, due to the presence of submarine slide breccias, intrabasinal turbidites, and slumps (Bersezio et al., 1993; Castellarin, 1972; Winterer and Bosellini, 1981). We suggest a possible post-rift E-W-trending extensional activity in the eastern Lombardian Basin, whose far-field effect caused deformation in the Amora Fault System area (Fig. 15b).

5.1.2. Alpine evolution

The boundary between the Early and Late Cretaceous was marked by the first evidence of syn-sedimentary activity associated with the onset of the Eoalpine orogeny at the Aptian–Albian transition (Berra and Carminati, 2009; Bersezio et al., 1993; Winterer and Bosellini, 1981). By the end of the Eoalpine compression, the present-day structure of the central Southern Alps (cSA) was largely exhumed, as indicated by thermochronological data that constrain the emplacement of magmatic bodies at shallow crustal levels (~2–4 km, above the Partial Annealing Zone) around 40 Ma (Bergomi et al., 2015; D'Adda et al., 2011; Malusà et al., 2011). These intrusions clearly crosscut major thrust faults in the northern sector of the cSA (D'Adda et al., 2011; Zanchetta et al., 2015).

At this stage, it is plausible that the Albino Thrust was already active as a S-verging structure, predating middle Eocene magmatism (Fig. 16a). This interpretation is supported by crosscutting relationships observed east of the Mt. Rena half-graben (Colle Gallo area, left hydrographic side of the Seriana Valley), where a S-verging thrust juxtaposes the Norian Zorzino Limestone and Riva di Solto Shale in the hanging wall on top of the Rhaetian Zu Limestone in the footwall. The Norian succession forms a south-verging syncline (Mt. Altino area) that is itself crosscut by mid-Eocene magmatic bodies (Bellotti et al., 2025; Bersezio et al., 2012; Forcella and Jadoul, 2000).

This structure occurs at a stratigraphic level different from that of the Albino Thrust, and the two are separated by a kilometre-scale, N–S-striking strike-slip fault, making their direct correlation uncertain. Nevertheless, both structures were likely active contemporaneously. Additionally, a magmatic body in the Colle Gallo area is displaced by a transpressive structure (Bellotti et al., 2025; Bersezio et al., 2012; Forcella and Jadoul, 2000), coinciding with a local bend in a secondary thrust fault. This deformation may reflect reactivation during the Oligocene N–S-oriented compressional phase (D_4). A similar configuration is observed in the Amora area, where an andesitic dike is crosscut by a secondary thrust fault (TF5, Figs. 9 and 11a, b).

From the Oligocene onward, compression resumed with the deformation front migrating in the frontal part of the belt (D_4; Zanchetta et al., 2015). The northern sector of the cSA was affected by a dextral

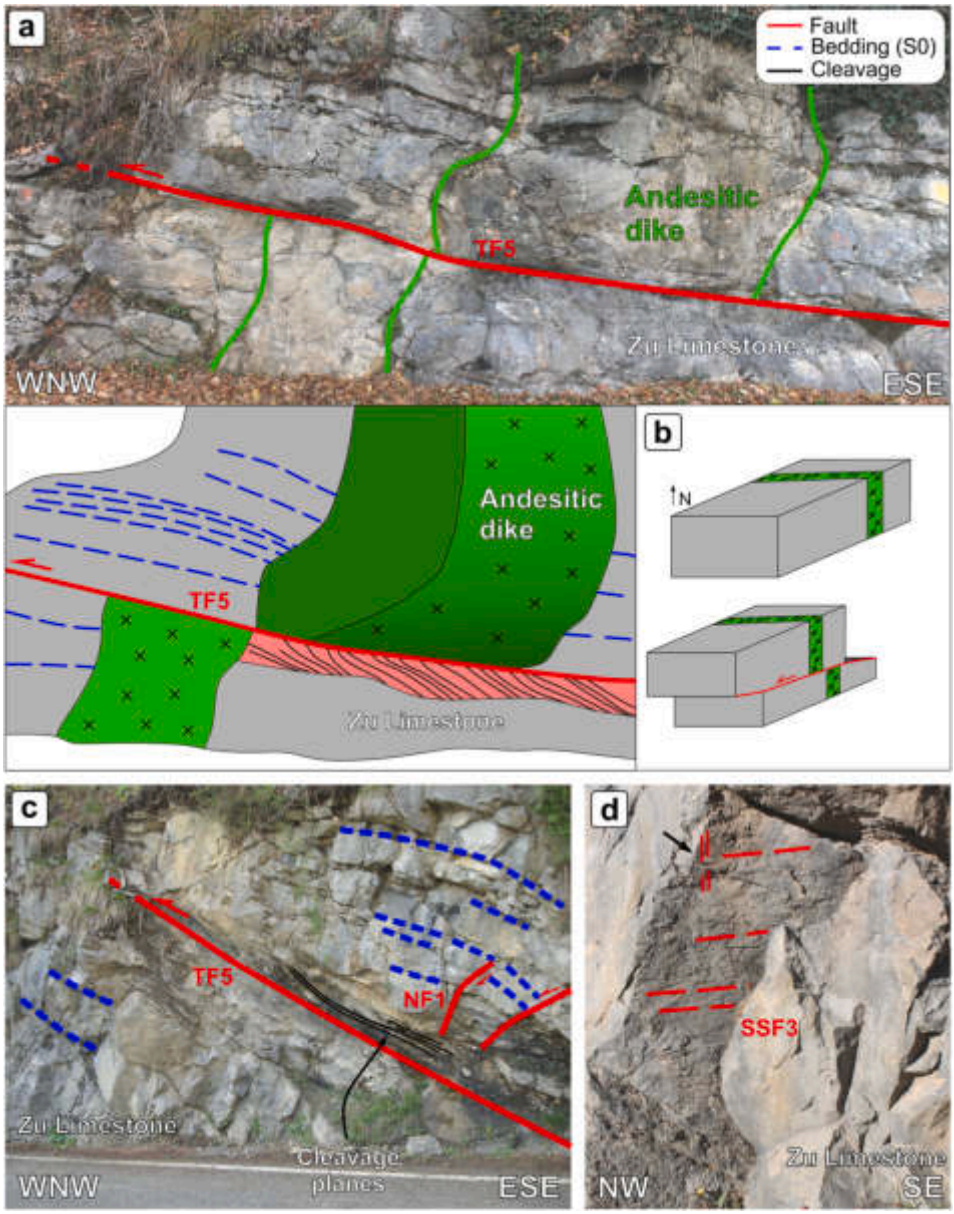

Fig. 11. Mesoscale structural analysis of Amora area. **(a)** Mesoscale thrust fault (TF5) off setting a mid-Eocene andesitic dike in the hanging wall of AF. **(b)** Sketch illustrating the displacement of the andesitic dike. **(c)** Meso-scale thrust fault (TF5) developed within a shale layer of the Zu Limestone, with tilted normal faults (NF1) in the hanging wall. A north-dipping, high-angle cleavage in the shales is consistent with the thrusting event. **(d)** Reactivated N–S trending fault with growth fibres showing left-lateral movement (SSF3). Low-angle fibres overprint dip-slip slickenfibres from an earlier normal faulting phase (black arrow). TF5, NF1, and SSF3 refer to fracture sets, as reported in Fig. 9.

transpressional regime along the Insubric Fault, with strike-slip reactivations observed along the Orobic-Porcile-Gallinera Thrust and the Tonale Line (Garzanti and Malusà, 2008; Mittempergher et al., 2021; S. M. Schmid et al., 1989; Stipp et al., 2004; Zanchetta et al., 2023).

During the Alpine compressional phases, the N–S-striking normal faults of the Amora Fault System were reactivated with strike-slip kinematics (Fig. 14). Most lateral displacement and associated deformation were likely accommodated during the Late Cretaceous–Paleocene phase (D_{3a}–D_{3b}; Zanchetta et al., 2015), with only minor reactivation during the Neogene post-collisional stage (D_4). The faults are cut to the north by the Clusone Fault, a major structure related to pre-Adamello tectonics (Fig. 2; D'Adda et al., 2011), further indicating early reactivation of the system. The middle Eocene andesitic dikes that crosscut the Amora Fault (Figs. 2 and 16b) exhibit minimal deformation, suggesting that most of the strike-slip offset occurred prior to dikes intrusion. In the Amora area, these tectonic stages are associated with the re-opening of N–S-trending V1c tension gashes, now sealed by carbonate cements. The reactivation of these features implies an E–W-trending σ_3 stress orientation in the footwall of the AF. Two explanations can be proposed: (1) a local sub-horizontal permutation of σ_2 and σ_3 during N–S compression, producing an E–W-oriented σ_3 and thus re-opening the N–S tension gashes; or (2) reactivation of Jurassic rift-related N–S faults with strike-slip kinematics, leading to the formation of a releasing bend. Figs. 14 and 16 present a summary of the tectonic stages that affected the Amora Fault System from the Early Cretaceous to the Miocene, integrating meso-scale structural and paleostress analyses.

The first stage (100–45 Ma, Fig. 16a) corresponds to D_{3a} and D_{3b} of Zanchetta et al., 2015, during which the S-verging Albino Thrust developed (TF3; Fig. 9), and N-S-striking inherited normal faults were reactivated as right- and left-lateral strike-slip faults (SSF3; Figs. 9 and 14). Mesoscale structural and paleostress analyses on major thrust faults in the cSA (Zanchetta et al., 2011, 2015; Zanchi et al., 2012) suggest a

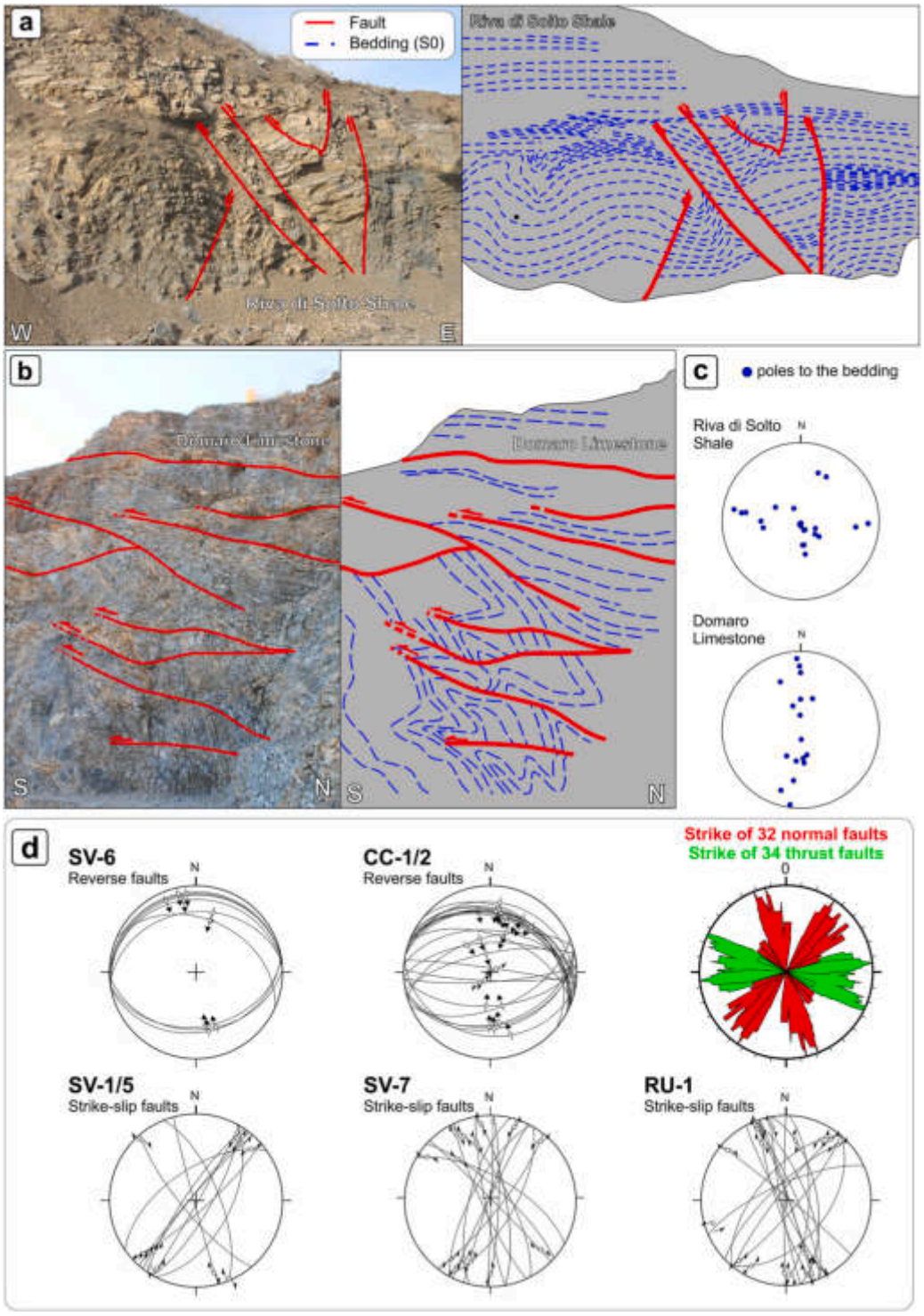

Fig. 12. **(a)** Folds and reverse faults in the Riva di Solto Shale forming the Dasla positive flower structure. Attitude of bedding planes are represented in the stereographic projection in **(c)**. Reverse faults originated from the reactivation of pre-existing normal faults formerly bounding a mesoscale graben. **(b)** S-verging folds and thrusts developed within the Domaro Limestone (CC-1/2), in the footwall of the Albino Thrust. Attitude of bedding planes are represented in the stereographic projection in **(c)**. **(d)** Structural data from fault planes in the Seriana Valley. Measurement sites are shown in Fig. 2. E–W-striking thrust faults (green) and N–S-striking strike-slip faults (red) are illustrated in the rose diagram. The strike-slip faults correspond to inherited normal faults reactivated during Alpine compression. (For interpretation of the references to colour in this figure legend, the reader is referred to the Web version of this article.)

NNW-SSE to NW-SE oriented σ_1 during this phase of Alpine compression, which aligns with the orientation of σ_1 observed along the Albino Thrust (SV-6; Fig. 14). The strike-slip reactivation of the Amora Fault System, however, suggests a slightly different σ_1 orientation, likely due to later reactivations overprinting earlier kinematic indicators or to local rotation of the stress field due to inherited structures.

In the second stage (43–38 Ma; Fig. 16b), E-W trending andesitic dikes were emplaced along E-W-striking normal faults (NF4; Fig. 14), resulting from an extensional stage with a N-S trending σ_3, consistent with the reconstruction by D'Adda et al. (2011).

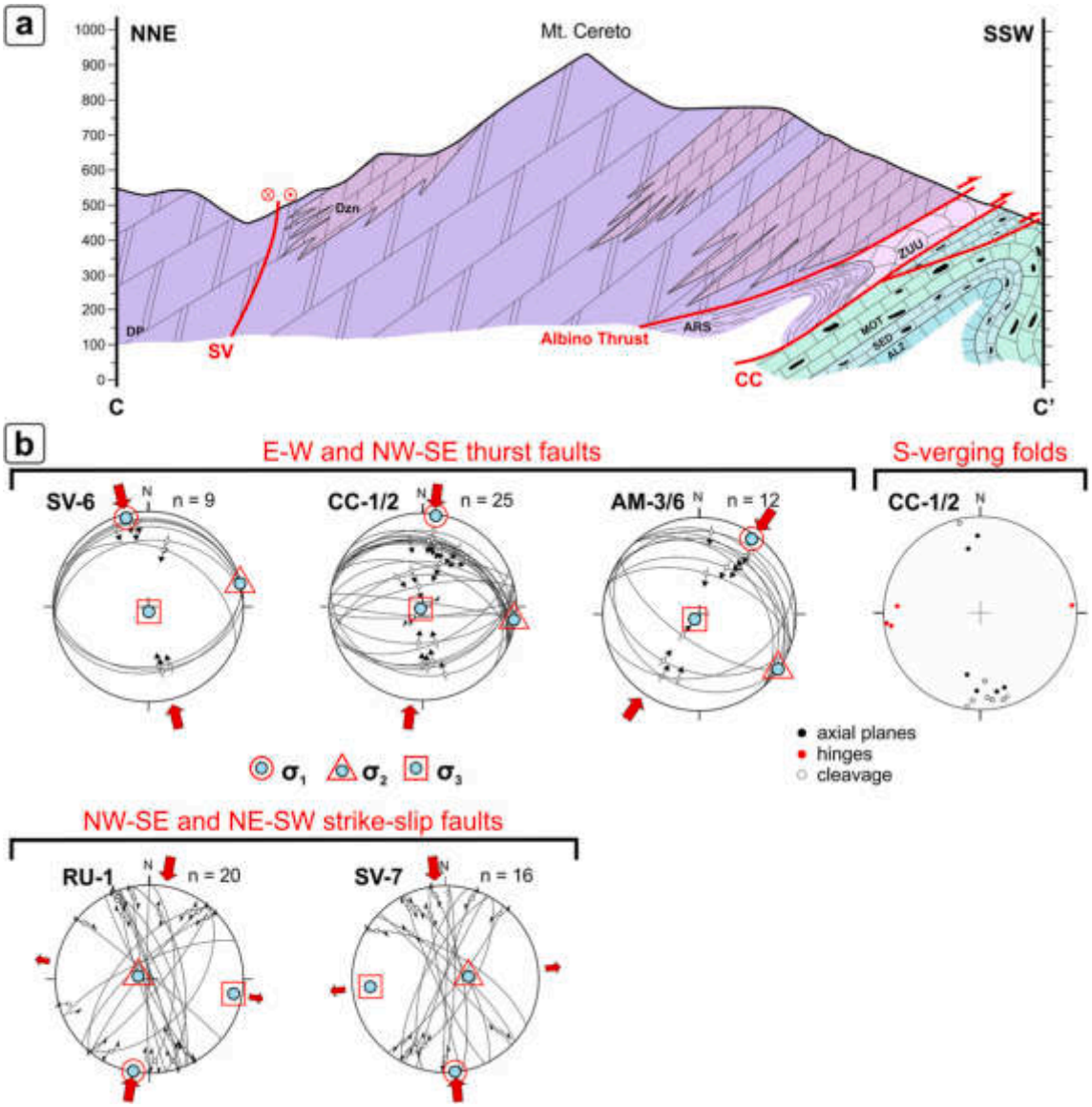

Fig. 13. **(a)** Cross section across the front of the Dolomia Principale thrust sheet. In the footwall of the Albino Thrust, S-verging folds affect the Norian–Lower Jurassic succession. The hanging wall is segmented by N–S-trending normal faults reactivated as left- and right-lateral strike-slip faults. **(b)** Thrust planes and folds from the front of the thrust sheet (SV-6 and CC-1/2), together with reactivated strike-slip faults (RU-1 and SV-7), indicate a N–S oriented compressional regime. Measurements from mesoscale thrust planes in the Amora area (AM-3/6) reveal a NE–SW-oriented σ_1 axis, likely reflecting a local stress variation. DP -Dolomia Principale; Dzn – Dolomie zonate; ARS – Riva di Solto Shale, ZUU – Zu Limestone; ALZ – Albenza Formation; SED – Sedrina Limestone; MOT – Moltrasio Limestone.

The third and final stage (36 Ma – present; Fig. 16b) corresponds to D_4 (Zanchetta et al., 2015). This stage is characterized by a further reactivation of N-S-striking normal faults as left- or right-lateral strike-slip faults and possibly renewed southward thrusting along the Albino Thrust. Paleostress inversion indicates a prevailing N-S trending σ_1 for both strike-slip faults (Fig. 14) and the secondary reverse faults. Similar σ_1 trends have been identified the entire Central Alps (Agliardi et al., 2009; Zanchetta et al., 2023).

It is worth noting that each tectonic stage was associated with paleo-fluids circulating through the fracture network sealing tension gashes, extensional veins and fault planes formed in response to tectonic stresses. The occurrence of different carbonate types, the difference of their habitus (e.g., blocky, fibrous, elongated-blocky) and luminescence, even within the same tectonic structure, points out to the interplay of several paleo-fluids. A careful geochemical and thermometric characterization of those cements could provide insights into the paleo-fluid provenance and the tectonic stage timing.

5.2. *The role of inherited structures during the Alpine orogeny*

5.2.1. *Extensional structures*

In a recent study, Samsu et al. (2023) discussed various ways in which pre-existing structures influence fault system geometry during basin formation in magma-poor rifts. Given that the Amora Fault System affected the upper continental crust and that the Jurassic rifting event in the cSA was dominated by faulting in a magma-poor setting (Beltrando et al., 2014; Manatschal, 2004, 2023; Mohn et al., 2011; Schaltegger et al., 2002), the concepts presented by Samsu et al. (2023) can be applied to this case study. Analogue models (e.g., Bellahsen and Daniel, 2005; Ghosh et al., 2020; Henza et al., 2010; Keep and McClay, 1997) and observations from natural multiphase rift systems (e.g., Bailey et al., 2005; Bell et al., 2014; Deng et al., 2017; Wu et al., 2023) demonstrate that when the extension direction changes during successive rifting phases, pre-existing faults influence rift geometry only if their orientation is favourable for reactivation. If the faults are not optimally oriented, new faults may form instead, while older faults may undergo

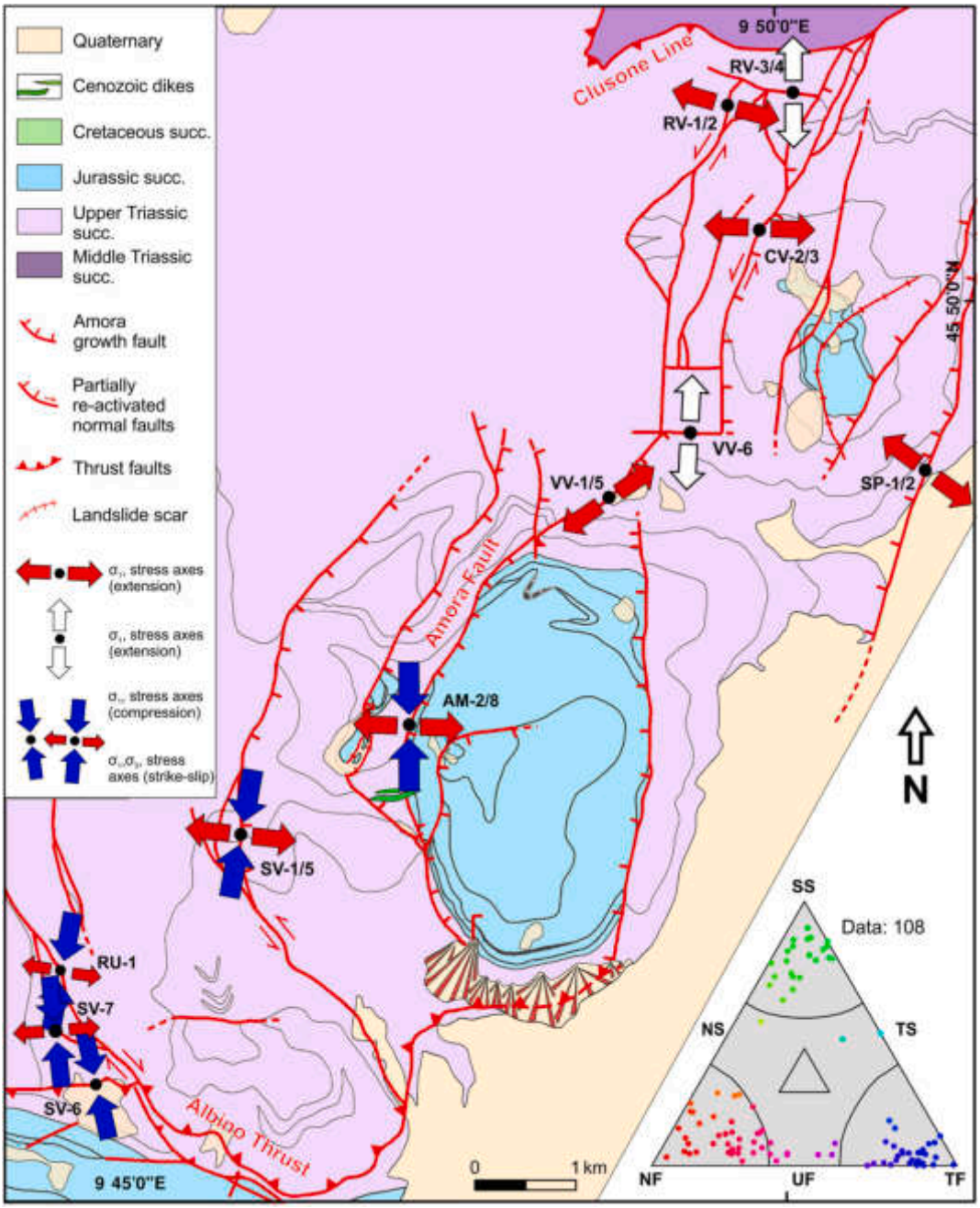

Fig. 14. Paleostress reconstruction along the AFS. Obtained paleostress solutions are reported for each site with trend and plunge of the main stress axes. Triangular Frolich diagrams are also shown. Frolich diagrams were obtained with Wintensor (Delvaux and Sperner, 2003).

oblique reactivation or remain inactive.

Another key factor influencing fault reactivation during multiphase rifting is thermal weakening. An example comes from the North Sea, where a N-S striking fault system developed during the Permian-Triassic rifting phase (Bell et al., 2014; Deng et al., 2017). During the major Middle Jurassic rifting episode, these older faults were not reactivated. Instead, new faults nucleated along the margins of a deep graben (North Viking Graben; Bell et al., 2014). Bell et al. (2014) linked the preferential initiation of these new faults to the rise and fall of the Middle Jurassic central North Sea thermal dome resulting in lithospheric weakening.

The thermal history of the Lombardian Basin has been investigated in several studies (Bersezio and Bellentani, 1997; Bertotti et al., 1999, 2001; Carminati et al., 2010; Ceriani et al., 2006; Fantoni and Scotti, 2003, among others), revealing high heat flow during the Jurassic rifting, with a thermal peak around the Aalenian-Bajocian time interval. The oldest age obtained from the damage zone of the Amora Fault is Early Jurassic (192.4 ± 1.7|8.4 Ma; Rocca et al., 2024), and evidence of syn-sedimentary activity is recorded in the Lower Jurassic deposits (Moltrasio Limestone, Figs. 4–6; Rocca et al., 2024). Based on this evidence, it can be inferred that the Amora Fault initiated as a new fault from the Early Jurassic.

The high heat flow may have played an important role favouring thermal weakening of the lithosphere, both during the Norian, and the Early Jurassic rifting stage. Strain was preferentially focused promoting the formation of new faults rather than reactivating older ones (Fig. 15a) – even if they were favourably oriented in an E-W-trending extension (Bell et al., 2014; Samsu et al., 2023). This is further supported by the orientation of Early Permian low-angle normal faults preserved in the northern part of the central Southern Alps (Aga-Vedello LANF; Locchi et al., 2022; Zanchi et al., 2019), which strike NE–SW and dip SSE at low

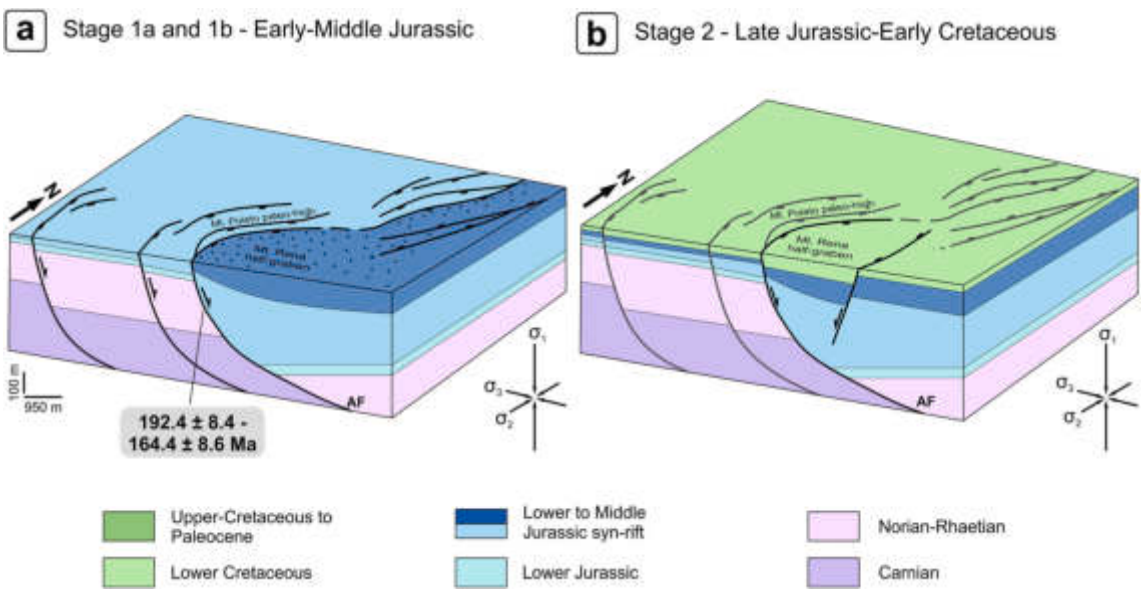

Fig. 15. Evolution of the Amora Fault System from Early Jurassic to Early Cretaceous. **(a)** The Lower Jurassic rifting event (Stage 1a) is characterized by activation of the N–S trending Amora Fault, along with syn-sedimentary deposition of Sinemurian Moltrasio Limestone within the Mt. Rena half-graben. The initiation of the AF was favoured over reactivation of inherited faults, likely due to elevated heat flow. Fault activity persisted until the end of the Middle Jurassic (Stage 1b). Geochronological data (*in-situ* U-Pb dating on calcite) are from Rocca et al. (2024). **(b)** The Late Jurassic–Early Cretaceous period involved renewed activity along the Amora Fault and reactivation of faults from previous rifting phases. This is evidenced by the preservation of the Lower Cretaceous sediments only within the subsiding Mt. Rena half-graben.

angles, in contrast to the Late Triassic–Early Jurassic N–S-striking high-angle normal faults. Therefore, during the subsequent Norian and Late Jurassic rifting stages, the formation of new faults was favoured over the reactivation of inherited ones, reflecting the first-order role of high heat flow in weakening the lithosphere (Bell et al., 2014; Mazzotti and Gueydan, 2018; Samsu et al., 2023).

After the thermal peak in Middle Jurassic, the heat flow rapidly decreased during the post-rift stage (Ceriani et al., 2006). During the Late Jurassic to Early Cretaceous, extensional activity resumed along the Ballino-Garda fault system (Bersezio et al., 1993; Castellarin, 1972; Winterer and Bosellini, 1981). Evidence of this stage can be found in the damage zone of the AF, where the antithetic eastern-bordering fault of the Mt. Rena half-graben – possibly inherited from the Norian rifting event – was reactivated. Its reactivation crosscut the Jurassic half-graben, reshaping it into a symmetric graben and increasing the displacement along the Amora Fault, as shown by the preservation of Lower Cretaceous sediments (Maiolica Formation) only within it (Fig. 15b). The reactivation can be linked to the favourable N-S orientation of the fault under an E-W-directed extensional regime, similar to fault reactivation observed in the North Sea (Bell et al., 2014; Deng et al., 2017).

The size and distribution of the inherited rift-related faults appear to control the localization of strain during subsequent faulting episodes (Bailey et al., 2005). An example comes from the fault population measured at stop SP-1/2, along a W-dipping fault bordering Mt. Cavlera and Mt. Rena (Fig. 2). Compared to other sites, a clockwise rotation of the σ_3 axis by more than 26° has been observed (Fig. 14). Berra and Jadoul (1996) documented a major E-dipping Norian syn-sedimentary fault marking the western boundary of the Iseo Basin, based on the juxtaposition of Carnian to Norian platform (Dolomia Principale), slope, and basin facies (Dolomie Zonate and Zorzino Limestone). It is likely that the SP-1/2 fault lies within the footwall damage zone of this Norian rift-related structure and was reactivated during the Jurassic rifting event. The observed variation in the principal stress axis orientation can be tentatively attributed to a rotation of the fault, or local irregularities, or to a sub-horizontal switch between σ_2 and σ_3, reflecting subtle but significant changes in the local stress regime driven by fault inheritance.

5.2.2. *Strike-slip tectonics*

From Late Cretaceous to Neogene, the Amora Fault System experienced strike-slip reactivations in response to N-S-directed Alpine compression. Strike-slip reactivation of normal faults is different from (a) a single-phase oblique extension or (b) a multi-phase extension where a first orthogonal extension is followed by an oblique extension (Rotevatn and Peacock, 2018, and citations herein).

Zones between adjacent normal faults segments typically display high intensity of irregularities and fractures. When such zones are reactivated as strike-slip faults, structural complexity increases significantly. Depending on the stepping direction of the original extensional faults and the reactivating strike-slip shear sense, the relay zone – the area between two fault segments – can become extensional (same-sense strike-slip reactivation) or contractional (opposite-sense strike-slip reactivation) (Cunningham and Mann, 2007; McClay and Bonora, 2001; Peacock, 2002; Peacock and Sanderson, 1994; Rotevatn and Peacock, 2018). Extensional domains have been more widely studied due to their effect on topography and sedimentation (e.g., Aydin and Nur, 1982; Childs et al., 1995; Crider and Pollard, 1998; Larsen, 1988; Mann et al., 1983; McClay and Dooley, 1995; Wu et al., 2009), whereas contractional strike-slip domains have been less frequently studied (e.g., Barton et al., 1998; Rotevatn and Peacock, 2018; Zampieri and Massironi, 2007).

The Mt. Rena half-graben basin is bounded to the west by three right-stepping N-S-striking faults reactivated with a left-lateral strike-slip shear sense (Fig. 14). This geometry likely caused localized shortening within the footwall of the Amora Fault, particularly across the Mt. Poieto–Nese structural high (Figs. 5–7). Mesoscale analysis in the Amora area reveals secondary thrust faults crosscutting mid-Eocene andesitic dikes (Fig. 11a), as well as evidence that many secondary normal faults in both hanging wall and footwall of the Amora Fault were reactivated as strike-slip faults (Figs. 5 and 6). These features indicate that shortening occurred prior to the emplacement of mid-Eocene intrusions, enhancing displacement along the Amora Fault and generating a positive paleotopographic relief in the Poieto–Nese area.

Further north along the Amora Fault System, two right-stepping, left-lateral strike-slip faults form a positive flower structure (DA-2; Figs. 12a

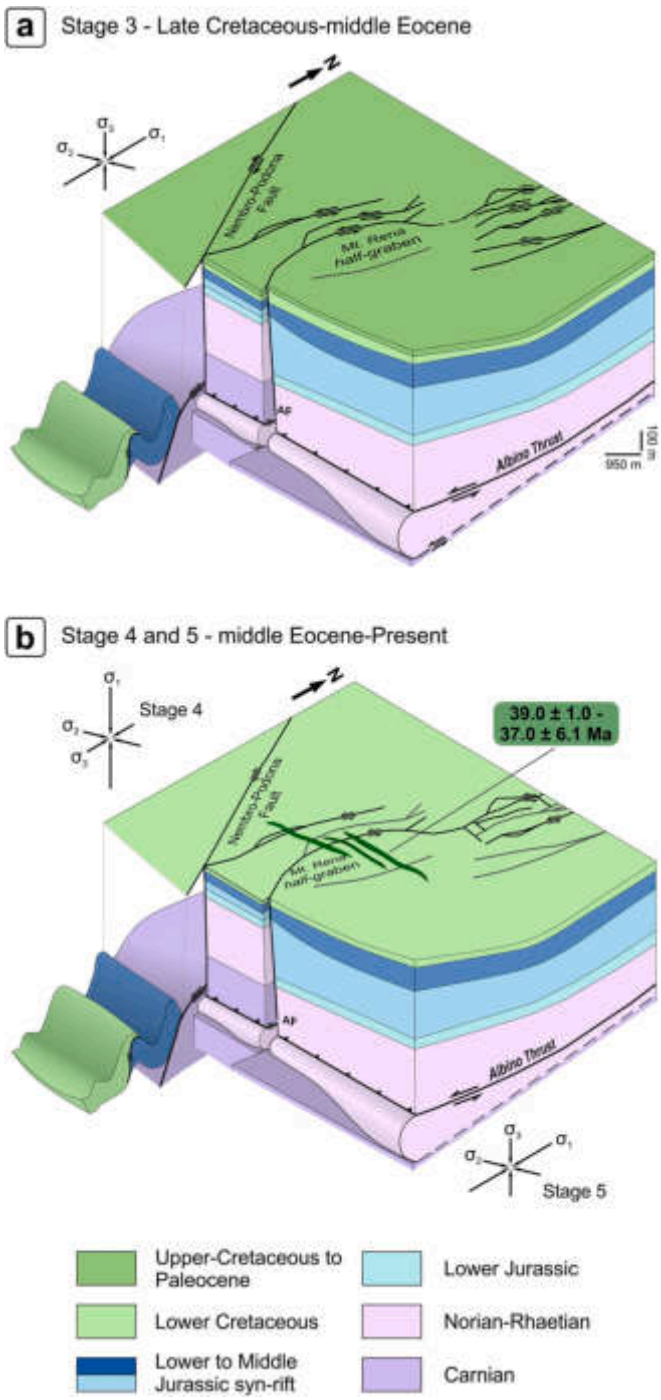

Fig. 16. Evolution of the Amora Fault System from Late Cretaceous to Present. **(a)** During the initial stages of Alpine compression (Late Cretaceous to mid-Eocene), the AFS was reactivated as a set of left- and right-lateral strike-slip faults, contemporaneous with S-verging thrusting along the Albino Thrust. The combination of opposite-sense strike-slip motions likely produced the arcuate geometry of the Albino Thrust. Additionally, right-lateral displacement along the Nembro–Podona Fault, together with the mechanically weak Norian–Rhaetian succession, contributed to the twist in the dip direction of the Albino Thrust. **(b)** E–W-trending normal faults with associated magmatic dikes crosscut the AFS during the middle Eocene. Geochronological data (U-Th-Pb dating of zircons and Apatite Fission Tracks data) are from D'Adda et al. (2011) and Bergomi et al. (2015). Subsequent minor strike-slip reactivations occurred from the Oligocene to the present during late Alpine compression.

and 14), likely reactivating a small Norian or Jurassic graben. Within this structure, the bedding of the Riva di Solto Shale is locally folded and offset by reverse faults, consistent with deformation under a N–S-oriented Alpine compression (Figs. 12a and 14). Several N-S-striking normal faults inherited from the Norian rifting event were reactivated with a strike-slip kinematic. Most display left-lateral motion, except for the NNW–SSEW-striking Nembro–Podona Fault (RU-1 and SV-7; Fig. 14), which was reactivated as a right-lateral fault due to its trend. Similar right-lateral motions were also observed for the Grem Line, north of the Clusone Fault (Zanchi et al., 2012). The combination of opposite-sense strike-slip movements likely contributed to the development of the complex arcuate geometry observed in the Albino Thrust zone (Figs. 2 and 14).

Another important factor influencing fault reactivation is the rheology of the involved rocks. Inherited normal faults represent zones of mechanical weakness, as they display different mechanical properties in respect with the undeformed surrounding rocks (Mandl, 1988; Brun and Nalpas, 1996; Del Ventisette et al., 2006; Bonini et al., 2012; Sieberer et al., 2023). Crustal-scale analogue models have shown that inherited faults and strength contrasts across platform–basin transitions strongly influence deformation patterns and structural architecture (Bonini et al., 2012; Brun and Nalpas, 1996; Del Ventisette et al., 2006; Mandl, 1988; Sieberer et al., 2023). Del Ventisette et al. (2006) investigated the relationship between the reactivation of pre-existing normal faults and the orientation of subsequent compressive stress fields. Their results demonstrated that the development of compressional structures is strongly influenced by the geometry of inherited faults and by the obliquity angle α (i.e., the angle between pre-existing faults and the principal compressive stress axis σ_1). Furthermore, a shallow décollement layer at the base of the graben significantly affects the deformation pattern within the sedimentary cover, leading to a decoupling between the basement and the syn-rift succession.

In the Amora Fault System, α values between reactivated normal faults and σ_1 derived from paleostress inversion range from ~0° to 14° (Fig. 14), consistent with the low-obliquity scenarios of Del Ventisette et al. (2006). In line with their findings, two main thrust décollements—orthogonal to the graben axis—developed at the lateral terminations of the Mt. Rena half-graben: the Clusone Fault to the north and the Albino Thrust to the south (Fig. 14). Strike-slip reactivation, typically left-lateral, is predicted under these conditions; however, the Nembro-Podona Fault exhibits right-lateral reactivation (Figs. 14 and 16a).This finds a counterpart in the model, where one of the graben-bounding faults is similarly reactivated as right-lateral, coinciding with a change in the dip direction of the lower-bordering thrust – from N-dipping to S-dipping (Fig. 17).

This behaviour was attributed to the rheological contrast promoted by the presence of a silicon layer at the base of the basin fill. A similar configuration is observed west of the Nembro-Podona Fault, where the Albino Thrust planes twists its dip direction from north-to south-dipping (Figs. 14, 16 and 17a; Zanchi et al., 1990). The base of the half-graben is filled by a weak Norian-Rhaetian succession (shales and marls) atop the Dolomia Principale Formation, which forms the rigid basement in analogue models (Sieberer et al., 2023). This contrast enabled decoupling between basement and cover, shaping the complex geometry of the Albino Thrust.

More recently, Sieberer et al. (2023) proposed several analogue models considering varying strength contrasts between platform and basins, as well as different obliquity angles of inversion (i.e., the angle between the shortening direction and the rift axes), to evaluate the role of pre-existing faults. Their findings further demonstrated that during inversion strain preferentially localizes along lateral rheological contrast, especially at platform–basin transitions, producing curved thrust fronts because of reduced mechanical strength of basin fills relative to adjacent platform units, and the structural inheritance of extensional faults. These features closely resemble the curved geometry of the Albino Thrust in the presence of the inherited extensional

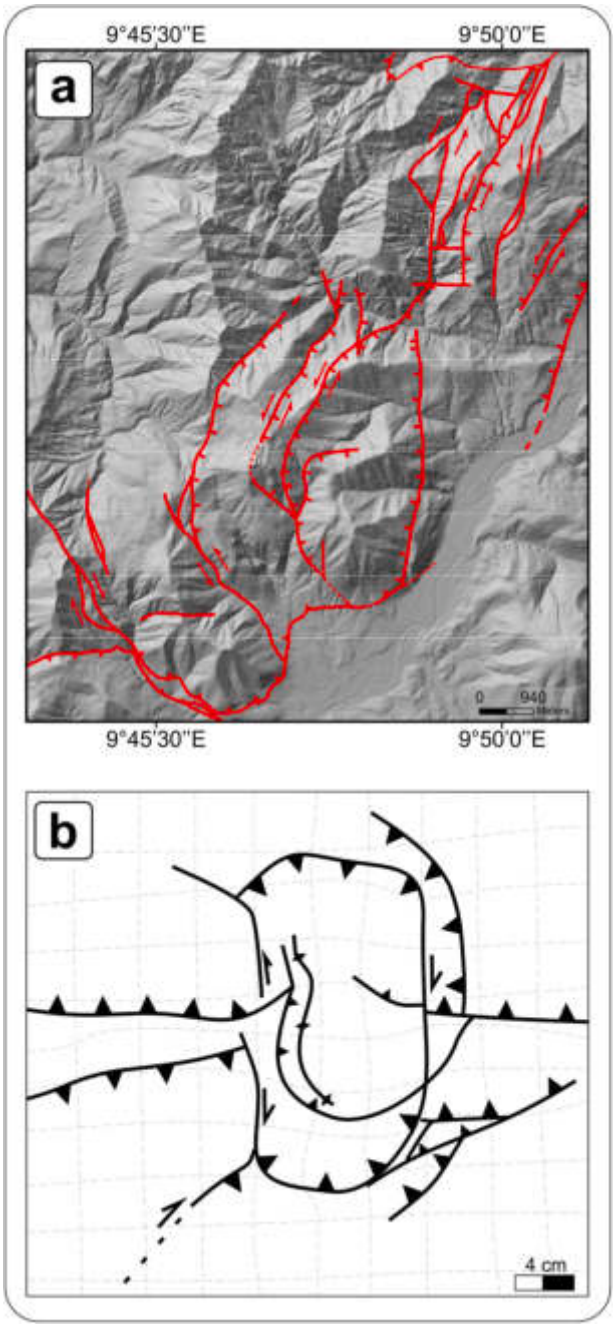

Fig. 17. Comparison between the AFS **(a)** and the Del Ventisette et al. (2006) model for α = 0° **(b)**. Both display a dip-direction twist of the lower thrust associated with reactivation of a pre-existing N–S-trending fault as right-lateral.

structures of the Amora Fault System, almost parallel to the direction of the Alpine compression.

Several studies have shown that inversion of inherited structures is responsible for modern moderate to large earthquakes (5.5 < M < 8.0) in diverse tectonic settings (e.g., Beauchamp et al., 1999; Chiaraluce et al., 2004; Ghisetti and Sibson, 2006; Jackson, 1980; Singh et al., 2016). This highlights the importance of understanding and quantifying the interplay between inherited fault architecture and increasing shortening, as this interaction can generate a wide range of inversion styles (Sibson and Ghisetti, 2018; Tarayoun et al., 2019).

Sibson and Ghisetti (2018) analysed dip angles of several inverted intracontinental faults associated with ruptures of M > 5.5. They observed that most fault dips (δ) conform to Anderson's fault theory (δ = 30° ± 5°), but that a subsidiary peak occurs at fault dips around δ = 50° ± 5°. In the context of compressional inversion, provided that the σ_1 stress trajectories remain horizontal, there is no expectation for a reverse fault to initiate with δ > 45°. Therefore, fault-slip ruptures with these dip angles are likely to involve reactivated inherited structures (Sibson and Ghisetti, 2018).

As discussed above, when α < 30°, these high-angle inherited faults are often reactivated as strike-slip structures (Del Ventisette et al., 2006; Rodríguez-Salgado et al., 2023). Consequently, the reactivation of inherited structures implies that, in some regions, they represent the dominant source of near-field seismic hazard. This interpretation is supported by the occurrence of modern Mw > 5.0 earthquakes caused by ruptures along inherited faults reactivated as strike-slip to oblique faults (e.g., the 1957 Gobi Altay earthquake, Mongolia, Mw = 7.8–8.0, Rizza et al., 2011; the 1969 Ceres–Tulbagh earthquake, South Africa, Mw = 6.3, Smit et al., 2015; the 2010–2011 Canterbury earthquake sequence, New Zealand, Mw = 6.2–7.0, Gledhill et al., 2011; the 1997 seismic sequence in Central Italy, Mw = 5–6, Chiaraluce et al., 2004).

Another important factor governing the competition between reactivation of pre-existing faults and the formation of new ones is the presence of fluid overpressure within and around fault zones (Sibson, 1992, 1995; Turner and Williams, 2004). Several studies (Collettini and Sibson, 2001; Leclère et al., 2012; Sibson and Ghisetti, 2018, among others) have shown that fluid overpressure favours re-shear along pre-existing faults, even when they are unfavourably oriented. Curzi et al. (2024) suggest that the 2016–2017 Central Apennines earthquakes may have been triggered by transient overpressures at depth (3–6 km), caused by an inherited thrust zone acting as a barrier to the migration of deep fluids.

Similarly, during the Late Cretaceous–early Eocene strike-slip reactivation of the Amora Fault System, the Albino Thrust may have acted as a fluid barrier. This behaviour was likely controlled by its geometry and by a clay-rich, multilayer carbonate succession within the deformation zone at comparable depths (~4–5 km, as inferred from apatite fission-track ages of mid-Eocene magmatic bodies; Zanchetta et al., 2015), promoting overpressure development and the upward release of fluids along high-angle strike-slip faults. The presence of circulating paleo-fluids is supported by carbonate slickenfibres on fault planes, as well as by the re-opening and carbonate sealing of tension gashes within the damage zone of the Amora Fault (Fig. S1). Several studies of mineral-filled deformation structures associated with fault activity (Agosta et al., 2008; Boullier and Robert, 1992; Cappa et al., 2009, among others) have revealed the presence of CO_2-rich hydrothermal fluids, highlighting the importance of studying these fault systems in the context of CO_2 storage and geothermal energy. In addition to their role in controlling fluid flow, N–S-striking inherited faults promote segmentation of the Albino Thrust, both within the study area and along its inferred lateral E–W continuations. Acting as transverse structures, they disrupt the lateral continuity of the thrust front and hinder the propagation of a single, through-going rupture (Sgambato et al., 2023). Similar segmentation of Alpine thrust fronts by transverse zones inherited from Mesozoic rift-related faults has been documented in the central Southern Alps (Faggio Line; Fiorini et al., 2025; Schönborn, 1992) and the Eastern Alps (Giudicarie Fault System; Zampieri et al., 2021). A comparable active example occurs in the Central Apennines, where the interaction between transverse structures and main faults resulted in a cascading sequence of earthquakes rather than a single large event (Schirripa Spagnolo et al., 2021).

In conclusion, the case of the Amora Fault System highlights the critical role of inherited pre-existing structures in shaping the deformation pattern during compression events. The reactivation of rift-related faults, combined with rheological contrasts, results in a complex and heterogeneous deformation pattern. This complexity is further enhanced when accounting for a history of multiphase rifting. Analogue models thus provide valuable insight into the relationships and relative chronology of such structures. At the same time, natural examples like

the Amora Fault System are essential for validating model predictions in geologically complex fault zones and for seismic hazard assessment, as they represent exhumed analogues of complex active fault systems whose investigation is often hindered by a lack of surface expression.

6. Conclusions

The Amora Fault System shows how inherited rift-related faults strongly influenced the structural and kinematic evolution of the central Southern Alps. Structural and paleostress analyses reveal a complex, multiphase tectonic history marked by repeated fault reactivations from the Jurassic rift to the Alpine orogeny, leading to the following conclusions.

1) The Amora Fault System experienced a polyphase tectonic evolution involving: (i) E-W-oriented long-lived Jurassic rift-related extension; (ii) E-W-oriented Late Jurassic post-rift extension with reactivation of basin-bordering faults; (iii) N-S-oriented Late Cretaceous–Middle Eocene Alpine compression, marked by activation of the S-verging Albino Thrust and strike-slip reactivation of normal faults; (iv) N-S-oriented mid-Eocene andesitic dike emplacement and extension; (v) renewed N-S-oriented compression and strike-slip reactivation especially of N-S-striking faults.
2) Tectonic stages (i) and (ii) were characterized by a vertical σ_1 and E–W-trending σ_3. Local clockwise rotation of the σ_3 axis ($\sim 26^\circ$) may reflect fault orientation and local irregularities. Stages (iii) and (v) indicate a N–S-oriented σ_1, with S-verging thrusts, folds, and reactivation of N–S-striking normal faults. The mid-Eocene magmatic event (stage iv) was marked by vertical σ_1 and N–S-trending σ_3.
3) Thermal conditions strongly influenced fault behaviour during rifting: high heat flow during rifting promoted a thermally weakened upper crust and the formation of new faults, while cooler post-rift conditions favoured reactivation of older structures.
4) During Alpine orogeny, the interplay of compressive stress orientation and mechanical contrasts led to both left- and right-lateral N-S-striking fault reactivations, strain partitioning, and the complex geometry of the Amora Fault System. Analogue models further demonstrate how complex thrust geometries can form along-strike, as observed along the Albino Thrust.
5) Modern moderate to large earthquakes frequently result from the reactivation of inherited fault systems—particularly high-angle rift-related structures reactivated as strike-slip or oblique faults, which control fluid flow and promote fault segmentation by transverse structures that limit rupture continuity—with the Amora Fault System providing a key exhumed natural example of how inherited structures govern deformation and near-field seismic hazard during compression.

This work emphasizes the critical role of inherited faults in shaping the evolution of mountain belts. It shows how multiphase fault reactivation, thermal conditions, and stress reorientation interact to produce complex structural patterns during orogenesis. These insights improve our understanding of fault reactivation processes, with broad implications for tectonic reconstruction, fluid flow pathways, and seismic hazard assessment.

CRediT authorship contribution statement

Martina Rocca: Writing – review & editing, Writing – original draft, Visualization, Methodology, Investigation, Formal analysis, Data curation, Conceptualization. **Stefano Zanchetta:** Writing – review & editing, Supervision, Methodology, Investigation, Funding acquisition. **Andrea Zanchi:** Writing – review & editing, Writing – original draft, Supervision, Methodology, Investigation, Funding acquisition, Data curation.

Declaration of competing interest

The authors declare the following financial interests/personal relationships which may be considered as potential competing interests: Stefano Zanchetta reports financial support was provided by Ministry of Education and Merit. If there are other authors, they declare that they have no known competing financial interests or personal relationships that could have appeared to influence the work reported in this paper.

Acknowledgements

This work has been financially supported by the Ministero dell'Università e della Ricerca (grant no. 2021- NAZ- 0299, CUP: J33C22000170001). We warmly acknowledge the support of L. Angiolini (University of Milan) in carrying out the stratigraphic logging. We are grateful to F. Berra (University of Milan) for valuable discussions that contributed to this work. The authors would like to thank Cugini S. p.A. for providing access to their quarry site and for their kind cooperation during the geological surveys. They also thank the Editor and the Editor-in-Chief for their editorial handling. The paper benefited from the useful suggestions of Dr. Manuel Curzi and an anonymous reviewer.

Appendix A. Supplementary data

Supplementary data to this article can be found online at https://doi.org/10.1016/j.jsg.2026.105650.

Data availability

Data will be made available on request.

References

Agliardi, F., Zanchi, A., Crosta, G.B., 2009. Tectonic vs. gravitational morphostructures in the central Eastern Alps (Italy): constraints on the recent evolution of the mountain range. Tectonophysics 474 (1–2), 250–270. https://doi.org/10.1016/j.tecto.2009.02.019.

Agosta, F., Mulch, A., Chamberlain, P., Aydin, A., 2008. Geochemical traces of CO_2 -rich fluid flow along normal faults in central Italy. Geophys. J. Int. 174 (2), 758–770. https://doi.org/10.1111/j.1365-246X.2008.03792.x.

Alsop, G.I., Marco, S., 2012. A large-scale radial pattern of seismogenic slumping towards the Dead Sea Basin. J. Geol. Soc. 169 (1), 99–110. https://doi.org/10.1144/0016-76492011-032.

Andrés, J., Alcalde, J., Ayarza, P., Saura, E., Marzán, I., Martí, D., et al., 2016. Basement structure of the Hontomín CO_2 storage site (Spain) determined by integration of microgravity and 3D seismic data. https://doi.org/10.5194/se-2016-13.

Angelier, J., Mechler, P., 1977. Sur Une Methode Graphique De Recherche Des Contraintes Principales Egalement Utilisables En Tectonique Et En Seismologie: La Methode Des Diedres Droits, S7-XIX, pp. 1309–1318.

Aydin, A., Nur, A., 1982. Evolution of pull-apart basins and their scale independence. Tectonics 1 (1), 91–105. https://doi.org/10.1029/TC001i001p00091.

Bailey, W.R., Walsh, J.J., Manzocchi, T., 2005. Fault populations, strain distribution and basement fault reactivation in the East Pennines Coalfield, UK. J. Struct. Geol. 27 (5), 913–928. https://doi.org/10.1016/j.jsg.2004.10.014.

Bally, A.W., 1983. Structural Styles and the Evolution of Sedimentary Basins. American Association of Petroleum Geologists.

Barton, C.M., Evans, D.J., Bristow, C.R., Freshney, E.C., Kirby, G.A., 1998. Reactivation of relay ramps and structural evolution of the Mere Fault and Wardour Monocline, northern Wessex Basin. Geol. Mag. 135 (3), 383–395. https://doi.org/10.1017/S0016756898008759.

Beauchamp, W., Allmendinger, R.W., Barazangi, M., Demnati, A., El Alji, M., Dahmani, M., 1999. Inversion tectonics and the evolution of the High Atlas Mountains, Morocco, based on a geological-geophysical transect. Tectonics 18 (2), 163–184. https://doi.org/10.1029/1998TC900015.

Bell, R.E., Jackson, C.A.-L., Whipp, P.S., Clements, B., 2014. Strain migration during multiphase extension: observations from the northern North Sea. Tectonics 33 (10), 1936–1963. https://doi.org/10.1002/2014TC003551.

Bellahsen, N., Daniel, J.M., 2005. Fault reactivation control on normal fault growth: an experimental study. J. Struct. Geol. 27 (4), 769–780. https://doi.org/10.1016/j.jsg.2004.12.003.

Bellotti, P., Bersezio, R., Zuffetti, C., 2025. Landscape evolution and aquifer building processes in a carbonate fold-and-thrust belt, Italian Southern Alps: insights from 3D geo-modelling. Earth Surf. Process. Landf. 50 (7), e70109. https://doi.org/10.1002/esp.70109.

Beltrando, M., Manatschal, G., Mohn, G., Dal Piaz, G.V., Vitale Brovarone, A., Masini, E., 2014. Recognizing remnants of magma-poor rifted margins in high-pressure

orogenic belts: the Alpine case study. Earth Sci. Rev. 131, 88–115. https://doi.org/10.1016/j.earscirev.2014.01.001.
Bergomi, M.A., Zanchetta, S., Tunesi, A., 2015. The tertiary dike magmatism in the Southern Alps: geochronological data and geodynamic significance. Int. J. Earth Sci. 104 (2), 449–473. https://doi.org/10.1007/s00531-014-1087-5.
Bernoulli, D., Winkler, W., 1990. Heavy Mineral Assemblages from Upper Cretaceous South- and Austroalpine Flysch Sequences (Northern Italy and Southern Switzerland): Source Terranes and Palaeotectonic Implications, vol. 83, pp. 287–310.
Bernoulli, D., Bertotti, G., Froitzheim, N., 1967. Mesozoic faults and associated sediments in the Austroalpine-South Alpine continental margin. Memor. Soc. Geol. Ital. 45, 25–38.
Berra, F., 2023. Soft-sediment deformation structures and Neptunian dykes across a carbonate system: evidence for an earthquake-related origin (Norian, Dolomia Principale, Southern Alps, Italy). Sedimentology 1–24.
Berra, F., Carminati, E., 2009. Subsidence history from a backstripping analysis of the Permo-Mesozoic succession of the Central Southern Alps (Northern Italy): subsidence history from backstripping analysis. Basin Res. 952–975. https://doi.org/10.1111/j.1365-2117.2009.00453.x.
Berra, F., Jadoul, F., 1996. Norian serpulid and microbial bioconstructions: implication for the platform evolution in the Lombardy Basin (Southern Alps, Italy). Facies 35 (1), 143–162. https://doi.org/10.1007/BF02536961.
Berra, F., Galli, M.T., Reghellin, F., Torricelli, S., Fantoni, R., 2009. Stratigraphic evolution of the Triassic-Jurassic succession in the Western Southern Alps (Italy): the record of the two-stage rifting on the distal passive margin of Adria. Basin Res. 21 (3), 335–353. https://doi.org/10.1111/j.1365-2117.2008.00384.x.
Berra, F., Jadoul, F., Anelli, A., 2010. Environmental control on the end of the Dolomia Principale/Hauptdolomit depositional system in the central Alps: coupling sea-level and climate changes. Palaeogeogr. Palaeoclimatol. Palaeoecol. 290 (1–4), 138–150. https://doi.org/10.1016/j.palaeo.2009.06.037.
Bersezio, R., Erba, E., Gorza, M., Caccialanza, R., 1994. Stratigraphy, swdimentology and organic geochemistry of the Lower Cretaceous black shales from the Lombardy Basin (Southern Alps, Northern Italy). Int. Ass. Sedimentologists, 15th Regional Meeting, Ischia 56–58.
Bersezio, R., Erba, E., Gorza, M., Riva, A., 2002. Berriasian–Aptian black shales of the Maiolica formation (Lombardian Basin, Southern Alps, Northern Italy): local to global events. Palaeogeogr. Palaeoclimatol. Palaeoecol. 180 (4), 253–275. https://doi.org/10.1016/S0031-0182(01)00416-3.
Bersezio, Riccardo, Bellentani, G., 1997. The thermal maturity of the Southalpine Mesozoic succession north of Bergamo, by vitrinite reflectance data. Atti Ticinensi Sci. della Terra 5, 101–114.
Bersezio, Riccardo, Fornaciari, M., Gelati, R., Napolitano, A., Valdisturlo, A., 1993. The Significance of the Upper Cretaceous to Miocene Clastic Wedges in the Deformation History of the Lombardian Southern Alps, vol. 69, pp. 3–20.
Bersezio, Riccardo, Felletti, F., Lozar, F., Ruggeri, M., 1996. The Concesio Formation of the Lombardian rifted basin (Southern Alps, Italy). Stratigraphy of a Jurassic calcareous turbidite unit. Riv. Ital. Paleontol. Stratigr. 102 (1), 49–64.
Bersezio, Riccardo, Jadoul, F., Chinaglia, N., 1997. Geological map of the Norian-Jurassic succession of the Southern Alps of Bergamo. An explenatory note 116, 363–378.
Bersezio, Riccardo, Felletti, F., Riva, S., Micucci, L., 2009. Trends in bed thickness and facies of turbiditic sandstone bodies: unravelling the effects of Basin confinement, depositional processes, and modes of sediment supply. In: External Controls on Deep-Water Depositional Systems, vol. 92. SEPM (Society for Sedimentary Geology). https://doi.org/10.2110/sepmsp.092.
Bersezio, Riccardo, Bini, A., Ferliga, C., Gelati, R., Beretta, G.P., Corbari, D., et al., 2012. Note Illustrative Della Carta geologica D'Italia Alla Scala 1:50.000. Foglio 098 - Bergamo, vol. 5. Regione Lombardia, ISPRA - System. Cart, Roma.
Bertotti, G., Seward, D., Wijbrans, J., Ter Voorde, M., Hurford, A.J., 1999. Crustal thermal regime prior to, during, and after rifting: a geochronological and modeling study of the Mesozoic South Alpine rifted margin. Tectonics 18 (2), 185–200. https://doi.org/10.1029/1998TC900028.
Bertotti, Giovanni, 1991. Early Mesozoic extension and Alpine shortening in the Western Southern Alps: the geology of the area between Lugano and Menaggio (Lombardy, Northern Italy). Mem. Sci. Geol. 53, 17–123.
Bertotti, Giovanni, 2001. Subsidence, deformation, thermal and mechanical evolution of the Mesozoic South Alpine rifted margin: an analogue for Atlantic-type margins. Geological Society 187 (1), 125–141. https://doi.org/10.1144/GSL.SP.2001.187.01.07. London, Special Publications.
Bertotti, Giovanni, Picotti, V., Bernoulli, D., Castellarin, A., 1993. From rifting to drifting: tectonic evolution of the South-Alpine upper crust from the Triassic to the Early Cretaceous. Sediment. Geol. 86 (1–2), 53–76. https://doi.org/10.1016/0037-0738(93)90133-P.
Bertrand, L., Jusseaume, J., Géraud, Y., Diraison, M., Damy, P.-C., Navelot, V., Haffen, S., 2018. Structural heritage, reactivation and distribution of fault and fracture network in a rifting context: case study of the western shoulder of the Upper Rhine Graben. J. Struct. Geol. 108, 243–255. https://doi.org/10.1016/j.jsg.2017.09.006.
Bonini, M., Sani, F., Antonielli, B., 2012. Basin inversion and contractional reactivation of inherited normal faults: a review based on previous and new experimental models. Tectonophysics 522–523, 55–88. https://doi.org/10.1016/j.tecto.2011.11.014.
Bons, P.D., Elburg, M.A., Gomez-Rivas, E., 2012. A review of the formation of tectonic veins and their microstructures. J. Struct. Geol. 43, 33–62. https://doi.org/10.1016/j.jsg.2012.07.005.
Boullier, A.-M., Robert, F., 1992. Palaeoseismic events recorded in Archaean gold-quartz vein networks, Val d'Or, Abitibi, Quebec, Canada. J. Struct. Geol. 14 (2), 161–179. https://doi.org/10.1016/0191-8141(92)90054-Z.
Brack, P., 1984. Geologie Der Intrusiva Und Rahmengesteine Des Südwest-Adamello (Nord-Italien). ETH Zurich. PhD Thesis.
Brack, Peter, 1981. Structures in the southwestern border of the Adamello intrusion (Alpi Bresciane, Italy). Schweizerische Mineralogische Und Petrographische Mitteilungen 61 (1), 37–49.
Brogi, A., 2008. Fault zone architecture and permeability features in siliceous sedimentary rocks: insights from the Rapolano geothermal area (Northern Apennines, Italy). J. Struct. Geol. 30 (2), 237–256. https://doi.org/10.1016/j.jsg.2007.10.004.
Brown, D., Alvarez-Marron, J., Biete, C., Kuo-Chen, H., Camanni, G., Ho, C., 2017. How the structural architecture of the Eurasian continental margin affects the structure, seismicity, and topography of the south central Taiwan fold-and-thrust belt. Tectonics 36 (7), 1275–1294. https://doi.org/10.1002/2017TC004475.
Brun, J., Nalpas, T., 1996. Graben inversion in nature and experiments. Tectonics 15 (3), 677–687. https://doi.org/10.1029/95TC03853.
Buchanan, J.G., Buchanan, P.G., 1995. Basin Inversion. Geological Society Special Publication, London UK.
Buiter, S.J.H., Pfiffner, O.A., Beaumont, C., 2009. Inversion of extensional sedimentary basins: a numerical evaluation of the localisation of shortening. Earth Planet Sci. Lett. 288 (3–4), 492–504. https://doi.org/10.1016/j.epsl.2009.10.011.
Butler, R.W.H., Tavarnelli, E., Grasso, M., 2006. Structural inheritance in mountain belts: an Alpine–Apennine perspective. J. Struct. Geol. 28 (11), 1893–1908. https://doi.org/10.1016/j.jsg.2006.09.006.
Callegaro, E., Brack, P., 2002. Geological Map of the Tertiary Adamello Batholith (Northern Italy): Explanatory Notes and Legend, vol. 54, pp. 19–49.
Cappa, F., Rutqvist, J., Yamamoto, K., 2009. Modeling crustal deformation and rupture processes related to upwelling of deep CO_2 -rich fluids during the 1965–1967 Matsushiro earthquake swarm in Japan. J. Geophys. Res. Solid Earth 114 (B10). https://doi.org/10.1029/2009JB006398, 2009JB006398.
Carminati, E., 2009. Neglected basement ductile deformation in balanced-section restoration: an example from the Central Southern Alps (Northern Italy). Tectonophysics 463 (1–4), 161–166. https://doi.org/10.1016/j.tecto.2008.09.042.
Carminati, E., Cavazza, D., Scrocca, D., Fantoni, R., Scotti, P., Doglioni, C., 2010. Thermal and tectonic evolution of the southern Alps (northern Italy) rifting: coupled organic matter maturity analysis and thermokinematic modeling. AAPG (Am. Assoc. Pet. Geol.) Bull. 94 (3), 369–397. https://doi.org/10.1306/08240909069.
Casati, P., Gaetani, M., 1968. Lacune nel Triassico Superiore e nel Giurassico del Canto Alto - monte di Nese (Prealpi Bergamasche). Boll. Soc. Geol. It. 87, 719–731.
Casati, P., Gnaccolini, M., 1967. Geologia delle Alpi Orobie occidentali. Riv. Ital. Paleontol. Stratigr. 73, 25–162.
Castellarin, A., 1972. Evoluzione paleotettonica sin-sedimentaria del limite tra "piattaforma veneta" e "bacino lombardo", a Nord di Riva del Garda. Giorn. Geol. 2 (28), 11–212.
Castellarin, A., Vai, G.B., Cantelli, L., 2006. The Alpine evolution of the Southern Alps around the Giudicarie faults: a Late Cretaceous to early Eocene transfer zone. Tectonophysics 414 (1–4), 203–223. https://doi.org/10.1016/j.tecto.2005.10.019.
Ceriani, A., Di Giulio, A., Fantoni, R., Scotti, P., 2006. Cooling in rifting sequences during increasing burial depth due to heat flow decrease. Terra Nova 18 (5), 365–371. https://doi.org/10.1111/j.1365-3121.2006.00700.x.
Chiaraluce, L., Amato, A., Cocco, M., Chiarabba, C., Selvaggi, G., Di Bona, M., et al., 2004. Complex normal faulting in the apennines thrust-and-fold Belt: the 1997 seismic sequence in central Italy. Bull. Seismol. Soc. Am. 94 (1), 99–116. https://doi.org/10.1785/0120020052.
Childs, C., Watterson, J., Walsh, J.J., 1995. Fault overlap zones within developing normal fault systems. J. Geol. Soc. (152), 535–549.
Collettini, C., Sibson, R.H., 2001. Normal faults, normal friction? Geology 29 (10), 927. https://doi.org/10.1130/0091-7613(2001)029<0927:NFNF>2.0.CO;2.
Cooper, M., Warren, M.J., 2020. Inverted fault systems and inversion tectonic settings. In: Regional Geology and Tectonics: Principles of Geologic Analysis. Elsevier, pp. 169–204. https://doi.org/10.1016/B978-0-444-64134-2.00009-2.
Cooper, M.A., Williams, G.D., De Graciansky, P.C., Murphy, R.W., Needham, T., De Paor, D., et al., 1989. Inversion tectonics — a discussion. Geological Society 44 (1), 335–347. https://doi.org/10.1144/GSL.SP.1989.044.01.18. London, Special Publications.
Corvò, S., Montemagni, C., Zanchetta, S., Langone, A., 2025. Intermittent brittle and ductile deformation as recorded by dating of ultramylonites and pseudotachylytes in extending Continental crust (Ivrea-Verbano Zone, Italy). Terra Nova 37 (5), 277–286. https://doi.org/10.1111/ter.12775.
Coward, M.P., Gillcrist, R., Trudgill, B., 1991. Extensional structures and their tectonic inversion in the Western Alps. Geological Society, London, Special Publications 56 (1), 93–112. https://doi.org/10.1144/GSL.SP.1991.056.01.07.
Crider, J.G., Pollard, D.D., 1998. Fault linkage: three-dimensional mechanical interaction between echelon normal faults. J. Geophys. Res. Solid Earth 103 (B10), 24373–24391. https://doi.org/10.1029/98JB01353.
Cunningham, W.D., Mann, P., 2007. Tectonics of strike-slip restraining and releasing bends. Geological Society, London, Special Publications 290 (1), 1–12. https://doi.org/10.1144/SP290.1.
Curzi, M., Zuccari, C., Vignaroli, G., Degl'Innocenti, S., Viola, G., 2023. Alpine transpression in the Passo Rolle area (Dolomites, Italy): new structural and paleostress constraints. Italian Journal of Geosciences 142 (2), 200–216. https://doi.org/10.3301/IJG.2023.12.
Curzi, M., Cipriani, A., Aldega, L., Billi, A., Carminati, E., Van Der Lelij, R., et al., 2024. Architecture and permeability structure of the Sibillini Mts. Thrust and influence upon recent, extension-related seismicity in the central Apennines (Italy) through fault-valve behavior. GSA Bulletin. https://doi.org/10.1130/B36616.1.

D'Adda, P., Zanchi, A., Bergomi, M., Berra, F., Malusà, M.G., Tunesi, A., Zanchetta, S., 2011. Polyphase thrusting and dyke emplacement in the central Southern Alps (Northern Italy). Int. J. Earth Sci. 100 (5), 1095–1113. https://doi.org/10.1007/s00531-010-0586-2.

Dávalos-Elizondo, E., Laó-Dávila, D.A., 2023. Structural analysis of fracture networks controlling geothermal activity in the northern part of the Malawi Rifted Zone from aeromagnetic and remote sensing data. J. Volcanol. Geoth. Res. 433, 107713. https://doi.org/10.1016/j.jvolgeores.2022.107713.

Del Ventisette, C., Montanari, D., Sani, F., Bonini, M., 2006. Basin inversion and fault reactivation in laboratory experiments. J. Struct. Geol. 28 (11), 2067–2083. https://doi.org/10.1016/j.jsg.2006.07.012.

Delvaux, D., Sperner, B., 2003. New aspects of tectonic stress inversion with reference to the TENSOR program. Geological Society, London, Special Publications 212 (1), 75–100. https://doi.org/10.1144/GSL.SP.2003.212.01.06.

Deng, C., Fossen, H., Gawthorpe, R.L., Rotevatn, A., Jackson, C.A.-L., FazliKhani, H., 2017. Influence of fault reactivation during multiphase rifting: the Oseberg area, northern North Sea rift. Mar. Petrol. Geol. 86, 1252–1272. https://doi.org/10.1016/j.marpetgeo.2017.07.025.

Dickson, J.A.D., 1966. Carbonate identification and genesis as revealed by staining. J. Sediment. Petrol. 36, 491–505.

Doglioni, C., Bosellini, 1987. Eoalpine and Mesoalpine Tectonics in the Southern Alps, vol. 76, pp. 735–754.

Ewing, T.A., Rubatto, D., Beltrando, M., Hermann, J., 2015. Constraints on the thermal evolution of the Adriatic margin during Jurassic continental break-up: U–Pb dating of rutile from the Ivrea–Verbano Zone, Italy. Contrib. Mineral. Petrol. 169 (4), 44. https://doi.org/10.1007/s00410-015-1135-6.

Fantoni, R., Scotti, P., 2003. Thermal record of the Mesozoic extensional tectonics in the Southern Alps. Atti Ticinensi Sci. della Terra 9, 96–101.

Fantoni, R., Bersezio, R., Forcella, F., 2004. Alpine structure and deformation chronology at the Southern Alps-Po Plain border in Lombardy. Boll. Soc. Geol. It. 123, 463–479.

Ferrando, S., Bernoulli, D., Compagnoni, R., 2004. The Canavese Zone (Internal Western Alps): a Distal Margin of Adria.

Fiorini, A., Luca, A., Tavani, S., Rocca, M., Zanchetta, S., Zanchi, A., et al., 2025. Pre- and syn-orogenic tectonic evolution of the transverse zones dissecting the Central Southern Alps (Lombardy, Italy). https://doi.org/10.5194/egusphere-egu25-3502.

Fonseca, J., 1988. The Sou Hills: a barrier to faulting in the central Nevada Seismic Belt. J. Geophys. Res. Solid Earth 93 (B1), 475–489. https://doi.org/10.1029/JB093iB01p00475.

Forcella, F., Jadoul, F., 2000. Carta Geologica Della Provincia Di Bergamo Alla Scala 1: 50,000 Con Relativa Nota Illustrativa. Provincia Di Bergamo, Bergamo.

Gaetani, M., 1975. Jurassic stratigraphy of the Southern Alps: a review. Earth Sci. Soc. Libyan Arab Republic, (Geology of Italy) 377–402.

Galli, M.T., Jadoul, F., Bernasconi, S.M., Weissert, H., 2005. Anomalies in global carbon cycling and extinction at the Triassic/Jurassic boundary: evidence from a marine C-isotope record. Palaeogeogr. Palaeoclimatol. Palaeoecol. 216 (3–4), 203–214. https://doi.org/10.1016/j.palaeo.2004.11.009.

Gallo, L.C., Tomezzoli, R.N., Cristallini, E.O., 2017. A pure dipole analysis of the G ondwana apparent polar wander path: paleogeographic implications in the evolution of P angea. G-cubed 18 (4), 1499–1519. https://doi.org/10.1002/2016GC006692.

Garzanti, E., Malusà, M.G., 2008. The Oligocene Alps: domal unroofing and drainage development during early orogenic growth. Earth Planet Sci. Lett. 268 (3–4), 487–500. https://doi.org/10.1016/j.epsl.2008.01.039.

Ghisetti, F.C., Sibson, R.H., 2006. Accommodation of compressional inversion in north-western South Island (New Zealand): old faults versus new? J. Struct. Geol. 28 (11), 1994–2010. https://doi.org/10.1016/j.jsg.2006.06.010.

Ghosh, S., Bose, S., Mandal, N., Laik, A., 2020. Mid-crustal ramping of the Main Himalayan Thrust in Nepal to Bhutan Himalaya: new insights from analogue and numerical experiments. Tectonophysics 782–783, 228425. https://doi.org/10.1016/j.tecto.2020.228425.

Gledhill, K., Ristau, J., Reyners, M., Fry, B., Holden, C., 2011. The Darfield (Canterbury, New Zealand) Mw 7.1 Earthquake of September 2010: a Preliminary Seismological Report. Seismol Res. Lett. 82 (3), 378–386. https://doi.org/10.1785/gssrl.82.3.378.

Gunter, W.D., Bachu, S., Benson, S., 2004. The role of hydrogeological and geochemical trapping in sedimentary basins for secure geological storage of carbon dioxide. Geological Society, London, Special Publications 233 (1), 129–145. https://doi.org/10.1144/GSL.SP.2004.233.01.09.

Harding, T.P., 1985. Seismic characteristics and identification of negative flower structures, positive flower structures, and positive structural inversion. AAPG (Am. Assoc. Pet. Geol.) Bull. 69. https://doi.org/10.1306/AD462538-16F7-11D7-8645000102C1865D.

Hecker, S., DeLong, S.B., Schwartz, D.P., 2021. Rapid strain release on the Bear River fault zone, Utah–Wyoming—The impact of preexisting structure on the rupture behavior of a new normal fault. Tectonophysics 808, 228819. https://doi.org/10.1016/j.tecto.2021.228819.

Heidbach, O., Rajabi, M., Cui, X., Fuchs, K., Müller, B., Reinecker, J., et al., 2018. The World Stress Map database release 2016: crustal stress pattern across scales. Tectonophysics 744, 484–498. https://doi.org/10.1016/j.tecto.2018.07.007.

Henza, A.A., Withjack, M.O., Schlische, R.W., 2010. Normal-fault development during two phases of non-coaxial extension: an experimental study. J. Struct. Geol. 32 (11), 1656–1667. https://doi.org/10.1016/j.jsg.2009.07.007.

Hitchon, B., Gunter, W.D., Gentzis, T., Bailey, R.T., 1999. Sedimentary basins and greenhouse gases: a serendipitous association. Energy Convers. 40, 825–843.

Homberg, C., Bergerat, F., Philippe, Y., Lacombe, O., Angelier, J., 2002. Structural inheritance and cenozoic stress fields in the Jura fold-and-thrust belt (France). Tectonophysics 357 (1–4), 137–158. https://doi.org/10.1016/S0040-1951(02)00366-9.

Jackson, J., 1980. Errors in focal depth determination and the depth of seismicity in Iran and Turkey. Geophys. J. Int. 61 (2), 285–301. https://doi.org/10.1111/j.1365-246X.1980.tb04318.x.

Jadoul, F., Galli, M.T., 2008. The Hettangian shallow water carbonates after the Triassic/Jurassic biocalcification crisis: the Albenza Formation in the Western Southern Alps. Riv. Ital. Paleontol. Stratigr. 114 (3). https://doi.org/10.13130/2039-4942/5911.

Jadoul, F., Berra, F., Frisia, S., 1992. Stratigraphic and paleogeographic evolution of a carbonate platform in an extentional tectonic regime: the example of the Dolomia Principale in Lombardia (Italy). Riv. Ital. Paleontol. Stratigr. 98 (1), 29–44.

Jadoul, F., Maserti, D., Cirilli, S., Berra, F., Claps, M., Frisia, S., 1994. Norian–Rhaetian stratigraphy and paleogeographical evolution of the Lombardy Basin (Bergamasc Alps). 15th IAS Regional Meeting, Ischia 38.

Jadoul, F., Forcella, F., Bini, A., Ferliga, C., 2000. Note Illustrative Della Carta Geologica Della Provincia Di Bergamo Alla Scala 1:50000. Provincia di Bergamo.

Jadoul, F., Berra, F., Bini, A., Ferliga, C., Mazzoccola, D., Papani, L., et al., 2012. Foglio 077 : Clusone : Carta geologica D'Italia Alla Scala 1:50000, vol. 10. ISPRA. Servizio Geologico d'Italia, Roma.

Kampman, N., Burnside, N.M., Shipton, Z.K., Chapman, H.J., Nicholl, J.A., Ellam, R.M., Bickle, M.J., 2012. Pulses of carbon dioxide emissions from intracrustal faults following climatic warming. Nat. Geosci. 5 (5), 352–358. https://doi.org/10.1038/ngeo1451.

Keep, M., McClay, K.R., 1997. Analogue modelling of multiphase rift systems. Tectonophysics 273 (3–4), 239–270. https://doi.org/10.1016/S0040-1951(96)00272-7.

Kim, Y.-S., Andrews, J.R., Sanderson, D.J., 2001. Reactivated strike–slip faults: examples from north Cornwall, UK. Tectonophysics 340 (3–4), 173–194. https://doi.org/10.1016/S0040-1951(01)00146-9.

Lacombe, O., Mazzoli, S., Von Hagke, C., Rosenau, M., Fillon, C., Granado, P., 2019. Style of deformation and tectono-sedimentary evolution of fold-and-thrust belts and foreland basins: from nature to models. Tectonophysics 767, 228163. https://doi.org/10.1016/j.tecto.2019.228163.

Larsen, P.-H., 1988. Relay structures in a Lower Permian basement-involved extension system, East Greenland. J. Struct. Geol. 10 (1), 3–8. https://doi.org/10.1016/0191-8141(88)90122-8.

Laubscher, H.P., 1985. Large scale, thin-skinned thrusting in the southern Alps: kinematic models. Geol. Soc. Am. Bull. 96, 710–718. https://doi.org/10.1130/0016-7606(1985)96<710:LTTITS>2.0.CO;2.

Le Pichon, X., Jellinek, M., Lenardic, A., Şengör, A.M.C., İmren, C., 2021. Pangea migration. Tectonics 40 (6). https://doi.org/10.1029/2020TC006585 e2020TC006585.

Leclère, H., Fabbri, O., Daniel, G., Cappa, F., 2012. Reactivation of a strike-slip fault by fluid over pressuring in the southwestern French-Italian alps: reactivation of a strike-slip fault. Geophys. J. Int. 189 (1), 29–37. https://doi.org/10.1111/j.1365-246X.2011.05345.x.

Locchi, S., Zanchetta, S., Zanchi, A., 2022. Evidence of early Permian extension during the Post-Variscan evolution of the central Southern Alps (N Italy). Int. J. Earth Sci. 111 (6), 1717–1738. https://doi.org/10.1007/s00531-022-02220-2.

Lyon, P.J., Boult, P.J., Hillis, R.R., Bierbrauer, K., 2007. Basement controls on fault development in the Penola Trough, Otway Basin, and implications for fault-bounded hydrocarbon traps. Aust. J. Earth Sci. 54 (5), 675–689. https://doi.org/10.1080/08120090701305228.

Malusà, M.G., Villa, I.M., Vezzoli, G., Garzanti, E., 2011. Detrital geochronology of unroofing magmatic complexes and the slow erosion of Oligocene volcanoes in the Alps. Earth Planet Sci. Lett. 301 (1–2), 324–336. https://doi.org/10.1016/j.epsl.2010.11.019.

Manatschal, G., 2004. New models for evolution of magma-poor rifted margins based on a review of data and concepts from West Iberia and the Alps. Int. J. Earth Sci. 93 (3). https://doi.org/10.1007/s00531-004-0394-7.

Manatschal, G., Chenin, P., Haupert, I., Masini, E., Frasca, G., Decarlis, A., 2022a. The importance of rift inheritance in understanding the early collisional evolution of the Western alps. Geosciences 12 (12), 434. https://doi.org/10.3390/geosciences12120434.

Manatschal, G., Chenin, P., Ghienne, J., Ribes, C., Masini, E., 2022b. The syn-rift tectono-stratigraphic record of rifted margins (part I): insights from the Alpine Tethys. Basin Res. 34 (1), 457–488. https://doi.org/10.1111/bre.12627.

Manatschal, G., Chenin, P., Ulrich, M., Petria, B., Morin, M., Ballay, M., 2023. Tectono-magmatic evolution during the extensional phase of a Wilson Cycle: a review of the Alpine Tethys case and implications for Atlantic- type margins. Italian Journal of Geosciences 142 (1), 5–27. https://doi.org/10.3301/IJG.2023.01.

Mandl, G., 1988. *Mechanics of Tectonic Faulting. Models and Basic Concepts* (Vol. Developments in Structural Geology). Elsevier, Amsterdam.

Mann, P., Hempton, M.R., Bradley, D.C., Burke, K., 1983. Development of pull-apart basins. J. Geol. 91 (5), 529–554. https://doi.org/10.1086/628803.

Manzocchi, T., Childs, C., Walsh, J.J., 2010. Faults and fault properties in hydrocarbon flow models. Geofluids 10 (1–2), 94–113. https://doi.org/10.1111/j.1468-8123.2010.00283.x.

Mattioli, E., Erba, E., 1999. Synthesis of calcareous nannofossil events in tethyan Lower and Middle Jurassic successions. Riv. Ital. Paleontol. Stratigr. 105 (3), 343–376.

Mazzotti, S., Gueydan, F., 2018. Control of tectonic inheritance on continental intraplate strain rate and seismicity. Tectonophysics 746, 602–610. https://doi.org/10.1016/j.tecto.2017.12.014.

McClay, K., Bonora, M., 2001. Analog models of restraining step overs in strike-slip fault systems. AAPG (Am. Assoc. Pet. Geol.) Bull. 85. https://doi.org/10.1306/8626C7AD-173B-11D7-8645000102C1865D.

McClay, K., Dooley, T., 1995. Analogue models of pull-apart basins. Geology 23 (8), 711. https://doi.org/10.1130/0091-7613(1995)023<0711:AMOPAB>2.3.CO;2.

Ménard, G., Molnar, P., 1988. Collapse of a Hercynian Tibetan Plateau into a late Palaeozoic European Basin and Range province. Letters to Nature 334, 235–237.
Mittempergher, S., Zanchi, A., Zanchetta, S., Fumagalli, M., Gukov, K., Bistacchi, A., 2021. Fault reactivation and propagation in the northern Adamello pluton: the structure and kinematics of a kilometre-scale seismogenic source. Tectonophysics 806, 228790. https://doi.org/10.1016/j.tecto.2021.228790.
Mohn, G., Manatschal, G., Masini, E., Müntener, O., 2011. Rift-related inheritance in orogens: a case study from the Austroalpine nappes in Central Alps (SE-Switzerland and N-Italy). Int. J. Earth Sci. 100 (5), 937–961. https://doi.org/10.1007/s00531-010-0630-2.
Morley, C.K., 1995. Developments in the structural geology of rifts over the last decade and their impact on hydrocarbon exploration. Geological Society, London, Special Publications 80 (1), 1–32. https://doi.org/10.1144/GSL.SP.1995.080.01.01.
Müller, W., Prosser, G., Mancktelow, N.S., Villa, I.M., Kelley, S.P., Viola, G., Oberli, F., 2001. Geochronological constraints on the evolution of the Periadriatic Fault System (Alps). Int. J. Earth Sci. 90 (3), 623–653. https://doi.org/10.1007/s005310000187.
Muttoni, G., Gaetani, M., Kent, D.V., Sciunnach, D., Angiolini, L., Berra, F., et al., 2009. Opening of the Neo-Tethys Ocean and the Pangea B to Pangea A transformation during the Permian. GeoArabia 14 (4), 17–48. https://doi.org/10.2113/geoarabia140417.
Pace, P., Domenica, A.D., Calamita, F., 2014. Summit low-angle faults in the Central Apennines of Italy: younger-on-older thrusts or rotated normal faults? Constraints for defining the tectonic style of thrust belts. Tectonics 33 (5), 756–785. https://doi.org/10.1002/2013TC003385.
Passchier, C.W., Trouw, R.A.J., 2005. Microtectonics, second ed. Springer Verlag.
Peacock, D.C.P., 2002. Propagation, interaction and linkage in normal fault systems. Earth Sci. Rev. 58 (1–2), 121–142. https://doi.org/10.1016/S0012-8252(01)00085-X.
Peacock, D.C.P., Sanderson, D.J., 1994. Displacement, segment linkage and relay ramps in normal fault zones. J. Struct. Geol. 13, 721–733.
Pennacchioni, G., 2005. Control of the geometry of precursor brittle structures on the type of ductile shear zone in the Adamello tonalites, Southern Alps (Italy). J. Struct. Geol. 27 (4), 627–644. https://doi.org/10.1016/j.jsg.2004.11.008.
Petti, F.M., Falorni, P., 2007. Maiolica, vol. 1. Carta Geologica d'Italia.
Pohl, F., Froitzheim, N., Obermüller, G., Tomaschek, F., Schröder, O., Nagel, T.J., et al., 2018. Kinematics and Age of syn-intrusive detachment faulting in the Southern alps: evidence for early Permian crustal extension and implications for the pangea A versus B controversy. Tectonics 37 (10), 3668–3689. https://doi.org/10.1029/2018TC004974.
Rizza, M., Ritz, J.-F., Braucher, R., Vassallo, R., Prentice, C., Mahan, S., et al., 2011. Slip rate and slip magnitudes of past earthquakes along the Bogd left-lateral strike-slip fault (Mongolia): slip rate and slip value along the Bogd Fault. Geophys. J. Int. 186 (3), 897–927. https://doi.org/10.1111/j.1365-246X.2011.05075.x.
Roberts, N.M.W., Holdsworth, R.E., 2022. Timescales of faulting through calcite geochronology: a review. J. Struct. Geol. 158, 104578. https://doi.org/10.1016/j.jsg.2022.104578.
Rocca, M., Zanchetta, S., Gasparrini, M., Mangenot, X., Berra, F., Deschamps, P., et al., 2024. U-Pb Carbonate Dating Reveals long-lived Activity of Proximal Margin Extensional Faults During the Alpine Tethys Rifting, vol. 36, pp. 347–357. https://doi.org/10.1111/ter.12717.
Rodríguez-Salgado, P., Childs, C., Shannon, P.M., Walsh, J.J., 2023. Influence of basement fabrics on fault reactivation during rifting and inversion: a case study from the Celtic Sea basins, offshore Ireland. J. Geol. Soc. 180 (1), jgs2022–j2024. https://doi.org/10.1144/jgs2022-024.
Ronchi, P., Jadoul, F., Ceriani, A., Di Giulio, A., Scotti, P., Ortenzi, A., Previde Massara, E., 2011. Multistage dolomitization and distribution of dolomitized bodies in early Jurassic carbonate platforms (Southern Alps, Italy). Sedimentology 58 (2), 532–565. https://doi.org/10.1111/j.1365-3091.2010.01174.x.
Rotevatn, A., Peacock, D.C.P., 2018. Strike-slip reactivation of segmented normal faults: implications for basin structure and fluid flow. Basin Res. 30 (6), 1264–1279. https://doi.org/10.1111/bre.12303.
Rowland, J.V., Sibson, R.H., 2004. Structural controls on hydrothermal flow in a segmented rift system, Taupo Volcanic Zone, New Zealand. Geofluids 4 (4), 259–283. https://doi.org/10.1111/j.1468-8123.2004.00091.x.
Samsu, A., Micklethwaite, S., Williams, J.N., Fagereng, Å., Cruden, A.R., 2023. Structural inheritance in amagmatic rift basins: manifestations and mechanisms for how pre-existing structures influence rift-related faults. Earth Sci. Rev. 246, 104568. https://doi.org/10.1016/j.earscirev.2023.104568.
Santantonio, M., Carminati, E., 2011. Jurassic rifting evolution of the Apennines and Southern Alps (Italy): parallels and differences. Geol. Soc. Am. Bull. 123 (3–4), 468–484. https://doi.org/10.1130/B30104.1.
Schaltegger, U., Desmurs, L., Manatschal, G., Müntener, O., Meier, M., Frank, M., Bernoulli, D., 2002. The transition from rifting to sea-floor spreading within a magma-poor rifted margin: field and isotopic constraints. Terra Nova 14 (3), 156–162. https://doi.org/10.1046/j.1365-3121.2002.00406.x.
Schirripa Spagnolo, G., Mercuri, M., Billi, A., Carminati, E., Galli, P., 2021. The segmented campo felice normal faults: seismic potential appraisal by application of empirical relationships between rupture length and earthquake magnitude in the central apennines, Italy. Tectonics 40 (7). https://doi.org/10.1029/2020TC006465 e2020TC006465.
Schmid, S.M., Aebli, H.R., Heller, F., Zingg, A., 1989. The role of the Periadriatic Line in the tectonic evolution of the Alps. Geological Society, London, Special Publications 45 (1), 153–171. https://doi.org/10.1144/GSL.SP.1989.045.01.08.
Schmid, Stefan M., Fügenschuh, B., Kissling, E., Schuster, R., 2004. Tectonic map and overall architecture of the Alpine orogen. Eclogae Geol. Helv. 97 (1), 93–117. https://doi.org/10.1007/s00015-004-1113-x.
Schönborn, G., 1990. A kinematic model of the western Bergamasc Alps, Southern Alps, Italy [Text/html,application/pdf,text/html]. Eclogae Geol. Helv. 83 (3), 665–682. https://doi.org/10.5169/SEALS-166607.
Schönborn, G., 1992. Kinematics of a transverse zone in the Southern Alps, Italy. In: McClay, K.R. (Ed.), Thrust Tectonics. Springer Netherlands, Dordrecht, pp. 299–310. https://doi.org/10.1007/978-94-011-3066-0_27.
Sgambato, C., Walker, J.P.F., Roberts, G.P., Mildon, Z.K., Meschis, M., 2023. Influence of fault System geometry and slip rates on the relative role of coseismic and interseismic stresses on earthquake triggering and recurrence variability. J. Geophys. Res.: Solid Earth. 128 (11). https://doi.org/10.1029/2023JB026496 e2023JB026496.
Sibson, R.H., 1992. Implications of fault-valve behaviour for rupture nucleation and recurrence. Tectonophysics 211 (1–4), 283–293. https://doi.org/10.1016/0040-1951(92)90065-E.
Sibson, Richard H., Ghisetti, F.C., 2018. Review: factors affecting the assessment of earthquake hazard from compressional inversion structure. Bull. Seismol. Soc. Am. 108 (4), 1819–1836. https://doi.org/10.1785/0120170375.
Sieberer, A.-K., Willingshofer, E., Klotz, T., Ortner, H., Pomella, H., 2023. Inversion of extensional basins parallel and oblique to their boundaries: inferences from analogue models and field observations from the Dolomites Indenter, European eastern Southern Alps. Solid Earth 14 (7), 647–681. https://doi.org/10.5194/se-14-647-2023.
Sieberer, A.-K., Willingshofer, E., Klotz, T., Ortner, H., Pomella, H., 2025. Control of inherited structures on deformation and surface uplift: Crustal-scale analogue modelling with implications for the European eastern Southern Alps. Tectonophysics 907, 230736. https://doi.org/10.1016/j.tecto.2025.230736.
Singh, A.P., Dorbath, C., Ravi Kumar, M., Kumar, S., Chaudhary, I., Kayal, J.R., 2016. Fault geometry of the M_w 7.7 Western India intraplate earthquake: constrained from double-difference tomography and fault-plane solutions. Bull. Seismol. Soc. Am. 106 (4), 1446–1460. https://doi.org/10.1785/0120150280.
Smit, L., Fagereng, Å., Braeuer, B., Stankiewicz, J., 2015. Microseismic activity and basement controls on an active intraplate strike-slip fault, Ceres–Tulbagh, South Africa. Bull. Seismol. Soc. Am. 105 (3), 1540–1547. https://doi.org/10.1785/0120140262.
Spalla, M.I., Gosso, G., 1999. Pre-Alpine tectonometamorphic units in the central Southern Alps: structural and metamorphic memory. Mem Sci Geol (Padova) (51), 221–229.
Sperner, B., Müller, B., Heidbach, O., Delvaux, D., Reinecker, J., Fuchs, K., 2003. Tectonic stress in the Earth's crust: advances in the World Stress Map project. Geological Society, London, Special Publications 212 (1), 101–116. https://doi.org/10.1144/GSL.SP.2003.212.01.07.
Sperner, Blanka, Zweigel, P., 2010. A plea for more caution in fault–slip analysis. Tectonophysics 482 (1–4), 29–41. https://doi.org/10.1016/j.tecto.2009.07.019.
Stipp, M., Fügenschuh, B., Gromet, L.P., Stünitz, H., Schmid, S.M., 2004. Contemporaneous plutonism and strike-slip faulting: a case study from the Tonale fault zone north of the Adamello pluton (Italian Alps). Tectonics 23 (3). https://doi.org/10.1029/2003TC001515, 2003TC001515.
Tarayoun, A., Mazzotti, S., Gueydan, F., 2019. Quantitative impact of structural inheritance on present-day deformation and seismicity concentration in intraplate deformation zones. Earth Planet Sci. Lett. 518, 160–171. https://doi.org/10.1016/j.epsl.2019.04.043.
Tavani, S., Mencos, J., Bausà, J., Muñoz, J.A., 2011. The fracture pattern of the Sant Corneli Bóixols oblique inversion anticline (Spanish Pyrenees). J. Struct. Geol. 33 (11), 1662–1680. https://doi.org/10.1016/j.jsg.2011.08.007.
Tavani, Stefano, Granado, P., Corradetti, A., Camanni, G., Vignaroli, G., Manatschal, G., et al., 2021. Rift inheritance controls the switch from thin- to thick-skinned thrusting and basal décollement re-localization at the subduction-to-collision transition. GSA Bulletin 133 (9–10), 2157–2170. https://doi.org/10.1130/B35800.1.
Tavani, S., Maresca, A., Carminati, E., Cavinato, G.P., Corradetti, A., Granado, P., Manatschal, G., Muñoz, J.A., 2025. Zipper tectonics in the Tyrrhenian-Apennines system: linking rift inheritance with thrusting, back-arc extension and crustal delamination. Earth Sci. Rev. 271, 105305. https://doi.org/10.1016/j.earscirev.2025.105305.
Tueckmantel, C., Fisher, Q.J., Manzocchi, T., Skachkov, S., Grattoni, C.A., 2012. Two-phase fluid flow properties of cataclastic fault rocks: implications for CO2 storage in saline aquifers. Geology 40 (1), 39–42. https://doi.org/10.1130/G32508.1.
Turner, J.P., 1997. Strike-slip fault reactivation in the Cardigan Bay basin. J. Geol. Soc. 154 (1), 5–8. https://doi.org/10.1144/gsjgs.154.1.0005.
Turner, J.P., Williams, G.A., 2004. Sedimentary basin inversion and intra-plate shortening. Earth Sci. Rev. 65 (3–4), 277–304. https://doi.org/10.1016/j.earscirev.2003.10.002.
Wang, L., Maestrelli, D., Corti, G., Zou, Y., Shen, C., 2021. Normal fault reactivation during multiphase extension: analogue models and application to the Turkana depression, East Africa. Tectonophysics 811, 228870. https://doi.org/10.1016/j.tecto.2021.228870.
Wedmore, L.N.J., Biggs, J., Williams, J.N., Fagereng, Å., Dulanya, Z., Mphepo, F., Mdala, H., 2020. Active fault scarps in Southern Malawi and their implications for the distribution of strain in incipient Continental rifts. Tectonics 39 (3). https://doi.org/10.1029/2019TC005834 e2019TC005834.
Weert, A., Ogata, K., Vinci, F., Leo, C., Bertotti, G., Amory, J., Tavani, S., 2024. Multiple phase rifting and subsequent inversion in the West Netherlands Basin: implications for geothermal reservoir characterization. Solid Earth 15 (2), 121–141. https://doi.org/10.5194/se-15-121-2024.
Winterer, E.L., Bosellini, A., 1981. Subsidence and sedimentation on Jurassic passive Continental Margin, Southern alps, Italy. AAPG (Am. Assoc. Pet. Geol.) Bull. 65. https://doi.org/10.1306/2F9197E2-16CE-11D7-8645000102C1865D.

Wu, J.E., McClay, K., Whitehouse, P., Dooley, T., 2009. 4D analogue modelling of transtensional pull-apart basins. Mar. Petrol. Geol. 26 (8), 1608–1623. https://doi.org/10.1016/j.marpetgeo.2008.06.007.

Wu, L., Shen, C., Paton, D.A., Hou, Y., Mortimer, E.J., Mei, L., et al., 2023. A rift-scale view at strain partitioning during multiphase rifting: insights from the Hailar Basin, northeast Asia. Basin Res. 35 (4), 1362–1385. https://doi.org/10.1111/bre.12757.

Zampieri, D., Massironi, M., 2007. Evolution of a poly-deformed relay zone between fault segments in the eastern Southern Alps, Italy. Geological Society, London, Special Publications 290 (1), 351–366. https://doi.org/10.1144/SP290.13.

Zampieri, Dario, Vannoli, P., Burrato, P., 2021. Geodynamic and seismotectonic model of a long-lived transverse structure: the Schio-Vicenza Fault System (NE Italy). Solid Earth 12 (8), 1967–1986. https://doi.org/10.5194/se-12-1967-2021.

Zanchetta, S., D'Adda, P., Zanchi, A., Barberini, V., Villa, I.M., 2011. Cretaceous-Eocene compression in the central Southern Alps (N Italy) inferred from 40Ar/39Ar dating of pseudotachylytes along regional thrust faults. J. Geodyn. 51 (4), 245–263. https://doi.org/10.1016/j.jog.2010.09.004.

Zanchetta, S., Garzanti, E., Doglioni, C., Zanchi, A., 2012. The Alps in the Cretaceous: a doubly vergent pre-collisional orogen. Terra Nova 24 (5), 351–356. https://doi.org/10.1111/j.1365-3121.2012.01071.x.

Zanchetta, S., Malusà, M.G., Zanchi, A.M., 2015. Precollisional development and Cenozoic evolution of the Southalpine retrobelt (European Alps). Lithosphere L466.1. https://doi.org/10.1130/L466.1.

Zanchetta, S., Montemagni, C., Mascandola, C., Mair, V., Morelli, C., Zanchi, A., 2023. The Meran-Mauls Fault: tectonic switching from compression to transpression along a restraining bend of the Periadriatic Fault. J. Struct. Geol. 172, 104878. https://doi.org/10.1016/j.jsg.2023.104878.

Zanchi, A., Chinaglia, N., Conti, M., De Toni, S., Ferliga, C., Tsegaye, A., et al., 1990. Analisi strutturale lungo il fronte della Dolomia Principale in bassa Val Seriana (Bergamo). Memor. Soc. Geol. Ital. 45, 83–92.

Zanchi, A., Berra, F., Mattei, M., R. Ghassemi, M., Sabouri, J., 2006. Inversion tectonics in central Alborz, Iran. J. Struct. Geol. 28 (11), 2023–2037. https://doi.org/10.1016/j.jsg.2006.06.020.

Zanchi, A., D'Adda, P., Zanchetta, S., Berra, F., 2012. Syn-thrust deformation across a transverse zone: the Grem–Vedra fault system (central Southern Alps, N Italy). Swiss J. Geosci. 105 (1), 19–38. https://doi.org/10.1007/s00015-011-0089-6.

Zanchi, A., Zanchetta, S., Berio, L., Berra, F., Felletti, F., Volpi, V., et al., 2019. Low-angle normal faults record early Permian extensional tectonics in the Orobic Basin (Southern Alps, N Italy). Italian Journal of Geosciences 138 (2), 184–201. https://doi.org/10.3301/IJG.2018.35.

Zanchi, A., Zanchetta, S., Berra, F., Mattei, M., Javadi, H.R., Montemagni, C., 2021. Cenozoic dextral shearing along the arusan sector of the great kavir–doruneh fault System (Central Iran). Tectonics 40 (11). https://doi.org/10.1029/2021TC006766 e2021TC006766.

Zanchi, A., Ravazzi, C., Cavallin, A., Deaddis, M., De Amicis, M., Arosio, T., et al., 2022. Interplay of Holocene surface faulting and climate in the Central Po Plain, Italy. Quat. Res. 107, 71–86. https://doi.org/10.1017/qua.2021.68.

Ziegler, P.A., 1987. Compressional intra-plate deformations in the Alpine foreland—an introduction. Tectonophysics 137, 1–4.